Characterisation of a proton exchange membrane electrolyser using electrochemical impedance spectroscopy

---

A dissertation presented to

The School of Electrical, Electronic and Computer Engineering

North-West University

In fulfilment of the requirements for the degree

Magister Ingeneriae

in Electrical and Electronic Engineering

by

Jan Hendrik Petrus van der Merwe

Supervisor: Dr. K.R. Uren

Co-supervisor: Prof. G. van Schoor

Co-supervisor: Dr. D.G. Bessarabov

November 2012

Potchefstroom Campus

SUMMARY

Hydrogen is a promising energy carrier and a possible replacement for fossil fuel energy sources in the future. Hydrogen has the highest energy content per unit weight of any known fuel. The proton exchange membrane (PEM) electrolyser is a promising technology to produce hydrogen by splitting water into hydrogen and oxygen. A fundamental characterisation study of the PEM electrolyser is necessary to improve the technology. The aim of this study is therefore to characterise a PEM electrolyser using electrochemical impedance spectroscopy (EIS).

EIS is a non-invasive technique which measures the response of a system by applying a small sinusoidal disturbance signal. The advantage of using EIS is that the technique has the ability to distinguish between the different electrochemical processes. The EIS technique can be applied while the PEM electrolyser is operated at normal conditions.

Models found in the literature were used to develop an equivalent circuit model in such a way that each component in the equivalent circuit model represents a process or component in the PEM electrolyser. The EIS experimental results are fitted to the equivalent circuit model using a non-linear least squares method.

The equivalent circuit model was verified by using other electrochemical techniques such as the polarisation curves and Tafel plots. The polarisation curve was used to verify the ohmic resistance of the PEM electrolyser. Tafel plots showed the same trend as the EIS results for the activation losses. Mass transfer losses were verified

by changing the anode gas diffusion media.

The most significant findings which forms part of the validation of the equivalent circuit model are that the equivalent circuit model is capable of characterising different membrane electrode assemblies (MEAs), it can indicate the optimum operating area and it can facilitate component optimisation.

But now, thus says the Lord, who created you, O Jacob, And He who formed you, O Israel: "Fear not, for I have redeemed you; I have called you by your name; You are Mine."

Isaiah 43:1

ACKNOWLEDGEMENTS

I want to thank Jesus Christ for leading the way in my life. All the glory to Him.

I am honoured to have Dr. Kenny Uren as my supervisor and Prof. George van Schoor as my co-supervisor. Thank you for all the support, help and time during this study. I have not only learned a lot about research but also about life.

I want to thank Elisna for her support, prayers and encouragement. Thank you for believing in me. I want to thank my family Gert, Lida, Nalet and Marie for always praying and giving me hope.

I would like to thank HySA Infrastructure for identifying the need for this study and for funding this research. I would also like to thank Dr. Dmitri Bessarabov for the support and granting me the opportunity to further my studies.

CONTENTS

LIST OF FIGURES

LIST OF TABLES

Abbreviations

AC	Alternating Current
DC	Direct Current
CPE	Constant Phase Element
DI	Deionised
DOE	Department of Energy
EIS	Electrochemical Impedance Spectroscopy
EW	Equivalent Weights
FFT	Fast Fourier Transform
FRA	Frequency Response Analyser
GDL	Gas Diffusion Layer
GDLs	Gas Diffusion Layers
HER	Hydrogen Evolution Reaction
HHV	Higher Heating Value
HOR	Hydrogen Oxidation Reaction
HySA	Hydrogen of South Africa
IrRuOx	Iridium-Ruthenium Oxide
LHV	Low Heating Value
MEA	Membrane electrode assembly
MCTS	MicroStructured Substrate
Mtoe	Million Tonnes of Oil Equivalent
NLLS	Non-Linear Least Squares
NSTF	Nano Structured Thin Film
ORR	Oxidation Reduction Reaction
PEMFC	Proton Exchange Membrane Fuel Cell
PEM	Proton Exchange Membrane
Pt	Platinum

CHAPTER 1

INTRODUCTION

1.1 Hydrogen as an energy carrier

The need for a new energy carrier is unavoidable because the world's primary energy source is not sustainable. A total of 81% of the global energy consumption originates from burning fossil fuels, leading to high levels of carbon dioxide [1]. The increase in energy demand will lead to a rapid rise of carbon dioxide levels which will exponentially cause negative effects on the environment [5]. This phenomenon has necessitated the search for cleaner alternative energy sources.

Hydrogen as an energy carrier is one of the most promising options. Hydrogen has the following unique qualities as an energy carrier [6]:

1. There is an abundance of raw hydrogen in water.
2. The efficiency of hydrogen production through water electrolysis is high.
3. Hydrogen can be converted to electricity by means of a fuel cell and it is environmentally clean since in its production, storage, transportation and end use it does not produce any pollutants.

An idealised hydrogen economy is one in which hydrogen is produced from renewable

energy sources such as solar or wind through water electrolysis as shown in figure 1.1. The electricity from renewable energy sources is used to produce hydrogen through water electrolysis. The energy can then be converted to electricity via a fuel cell.

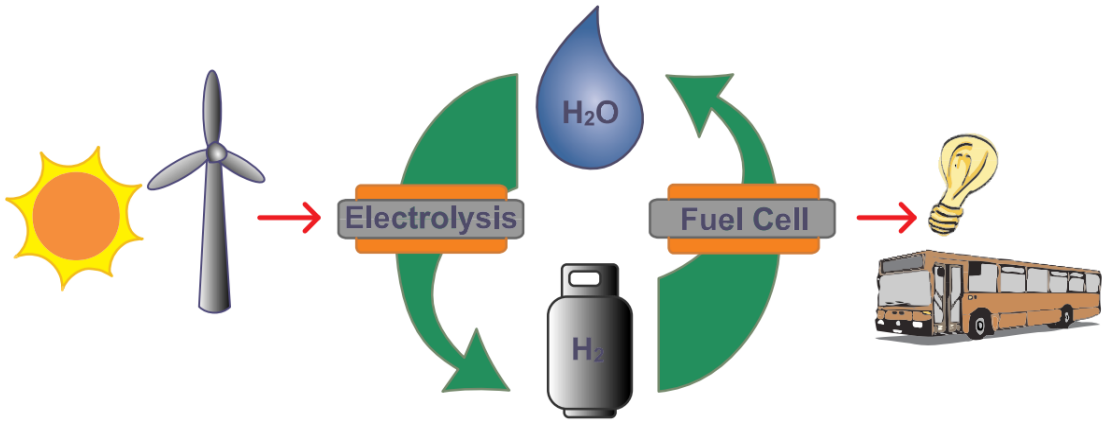

Figure 1.1: Ideal hydrogen energy cycle [1]

Although the electricity can be used directly from the renewable source the disadvantage of renewable energy sources like wind and solar is the fluctuation of geographical factors. The excess production of electricity by wind and solar during peak times should be stored and used when the renewable energy source is limited. The energy can be stored in many ways such as high energy super capacitors, fly wheels, lead acid batteries, li-ion batteries, flow batteries, compressed air, pumped hydro or hydrogen. Figure 1.2 shows a comparison of the energy storage technologies.

The amount of energy and storage time will determine which energy storage technology to use. Figure 1.2 shows that hydrogen is the preferred storage technology when large amounts of energy need to be stored for short and long periods of time [7].

1.2 Hydrogen production

Hydrogen can be produced in many ways including steam reforming, water electrolysis, photochemical reactions and biological processes. This study will focus on water electrolysis. The advantages of water electrolysis over the other hydrogen

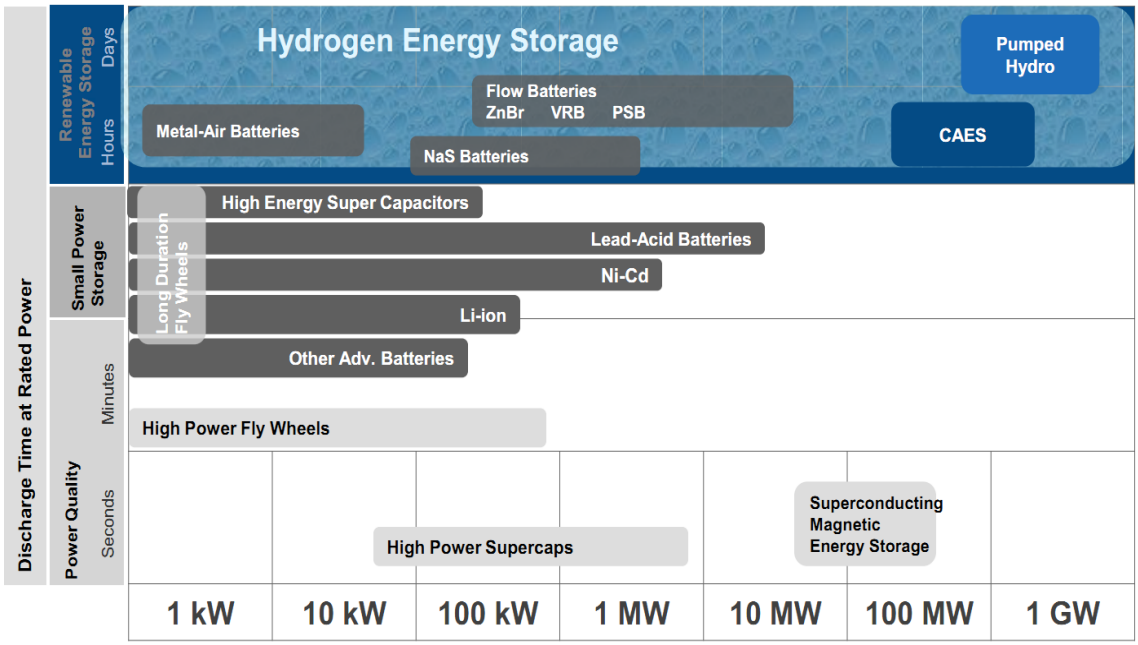

Figure 1.2: Energy storage technologies [2]

production methods are no carbon emissions, pure hydrogen, small scale possibilities and a efficient storage solution for the excess energy produced by renewable energy sources.

Hydrogen production from water electrolysis dates back to 1800 when William Nicholson and Anthony Carlisle discovered the electrolytical splitting of water [2]. The hydrogen production from water electrolysis grew rapidly and by 1902 more than 400 industrial electrolysers were in operation. The first hydrogen plant to produce 10,000 Nm^3/hr hydrogen was built in 1939.

Hydrogen is used in many applications in industry and as a result multiple markets exist. Today, there exist a number of mobile and stationary hydrogen power plants. These power plants are used for backup power in remote areas and in the telecommunication industry. The use of hydrogen in the automotive industry is also an upcoming technology.

Hydrogen is the fastest growing industrial gas for example power plants use hydrogen to cool the electric power generators. There are more than 16000 hydrogen-cooled generators worldwide, with a estimated market value of over $2 billion [8].

Hydrogen is also used in the electronics industry particularly in the manufacturing of semiconductors [7]. Food processing is another typical example where hydrogen is used.

The automotive industry had a growth from 80 million vehicles in 1950 to 900 million vehicles in 2000. The pollution associated when crude oil is burned and the scarcity of oil lead to the fuel cell automotive industry. Daimler announced market introduction of their fuel cell car by 2014. Toyota, GM, Honda and Hyundai will follow by manufacturing fuel cell cars by 2015 [7, 9]. An infrastructure for hydrogen filling stations needs to be addressed.

In summary it can be concluded that hydrogen is used in many industries and the demand for hydrogen is increasing. The production of hydrogen in this study is limited to the electrolysis of water. Electrolysis of water is a process in which the water is decomposed. Electrolysers are devices that perform water electrolysis.

Three types of electrolysers exist:

1. PEM electrolysers
2. Alkaline electrolysers
3. Solid Oxide electrolysers

Table 1.1 shows the operating temperatures of the electrolysers. PEM electrolysers provide advantages over alkaline and solid oxide electrolysers. A PEM electrolyser produces no harmful emissions (only water and hydrogen), it is compact, has a high production rate, is efficient and has a high degree of hydrogen purity [10]. The disadvantage of PEM electrolyser is the high capital cost.

HySA (Hydrogen of South Africa) is currently busy with research on hydrogen technology. The catalyst used in the hydrogen conversion process is platinum. 75% of the world's resources of platinum are estimated to be in South Africa [11]. The purpose of HySA is to add value to the platinum group metals (PGM) before it is exported. HySA Infrastructure at the North-West University is responsible for the infrastructure

Table 1.1: Types of Electrolysers

Type of electrolyser	**Operating temperature**
PEM	60 - 80°C
Alkaline	100 - 150°C
Solid Oxide	500 - 800°C

of hydrogen. The production of hydrogen, storage and transportation are important factors to establish an infrastructure. This study is part of the production of hydrogen and HySA Infratructure identified the need to characterise a PEM electrolyser.

1.3 Electrochemical characterisation techniques

Electrochemistry is the study of chemical changes caused by the flow of an electric current and the production of electrical energy caused by chemical reaction. Many techniques have been developed to characterise electrochemical systems [12].

Polarisation curves are most commonly used to measure the performance of an electrochemical cell. In a polarisation curve the voltage change is measured with a change in current density.

The current interruption method is used to measure the membrane resistance of a electrochemical cell. The principle of the method lies in the immediate change of current.

Cyclic voltammetry can provide rapid information about the electrochemical reactions. The potential is linearly scanned from initial to a vertex point and then the scan is reversed.

Electrochemical impedance spectroscopy (EIS) is an effective technique where the results can be converted to an equivalent circuit. Each component of the equivalent circuit gives information about the electrochemical reactions.

1.4 Problem statement

The purpose of this study is to characterise a PEM electrolyser. The losses associated with the electrochemical processes will be investigated. Electrochemical impedance spectroscopy is implemented and an equivalent circuit model is developed.

1.4.1 Scope

The scope of this study is to derive an equivalent circuit model which represents the PEM electrolyser. The hardware development is not part of this study and commercially available hardware and MEAs will be used, although the performances of the cell hardware and MEAs will be investigated. EIS is the selected electrochemical technique to develop an equivalent circuit model. Polarisation curves and Tafel plots will be used to verify the results.

1.5 Issues to be addressed and methodology

The characterisation of the PEM electrolyser can be divided into two sections, the experimental procedure and model development. Figure 1.3 displays a process flow diagram for this study.

The experimental procedure and model development will be performed at the same time and is discussed in chapter 4. This is due to the fact that the experimental results will be fitted to the equivalent circuit model and the development of the model is dependant on the EIS results. A non-linear least squares (NLLS) fitting method is used to fit the data of the equivalent circuit model to the experimental EIS data.

The parameter values of the equivalent circuit model are used to characterised the PEM electrolyser. The equivalent circuit model is verified by applying other electrochemical methods and getting the same results. The validation of the equivalent circuit model includes the characterisation of different membrane electrode assemblies (MEAs),

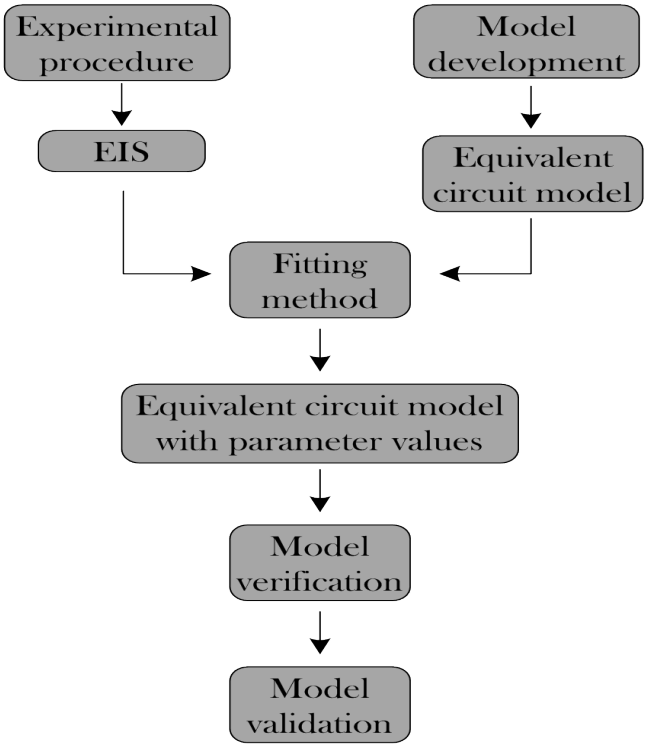

Figure 1.3: Outline of the study

identifying the optimum operating area and characterising electrolyser components.

1.5.1 Experimental procedure

The first step in the experimental procedure is to assemble the electrolyser and develop a test station. The assembly includes the structure, flow fields, gas diffusion layers (GDLs), gaskets and an MEA. The experimental test station includes the water supply and heating, separators, power supplies, frequency response analysers (FRA), galvanostats, potensiostats and temperature sensors.

The next step is to collect experimental data from the electrolyser. EIS data is collected while the experiment is operating at steady state condition, while a specific procedure is applied to collect data for the polarisation curves.

1.5.2 Model development

The next issue that need to be addressed is the development of an equivalent circuit model. The impedance data of the electrolyser is analysed and used to construct an equivalent circuit with the same impedance spectrum as the PEM electrolyser. This equivalent circuit model represents the electrolyser. The sub-objectives are the equivalent circuit components and impedance analysis.

1.5.3 Model verification and validation

The last step is to simulate the equivalent circuit model and verify the results with the impedance of the EIS data. The link between different chemical phenomena and the equivalent circuit components are necessary to analyse the performance of the electrolyser. The validation of the equivalent circuit model include the characterisation of three different MEAs, indication of the optimal operating point and characterising PEM electrolyser components.

1.6 Outline of the dissertation

Chapter 2 presents a literature study of the PEM electrolyser. The operation of a basic PEM electrolyser is explained. The theoretical models and equivalent models are discussed. A literature review shows previous work on PEM electrolyser analysis and approaches followed by previous researchers to characterise PEM fuel cells and electrolysers.

Chapter 3 describes the EIS method, which will be used to characterise the PEM electrolyser. Other methods like current interrupt and polarisation curves are considered. EIS is selected as the electrochemical method and the fundamentals of the method are discussed. Nyquist plots are used as a visual illustration of the impedance spectrum. The impedance of the components of the equivalent circuit are derived. The advantages of EIS are stated at the end of the chapter.

The characterisation procedure is the focus of chapter 4. The electrolyser setup includes the assembly of the PEM electrolyser and the necessary equipment to perform EIS is described. An equivalent circuit model is developed by using a basic Randles cell and adding different phenomena. The experimental data is fitted to the equivalent circuit model with a NLLS fitting algorithm.

Chapter 5 describes the verification of the equivalent circuit model. The ohmic, activation and mass transfer losses are characterised by EIS. The polarisation curve verified ohmic resistance results. The verification of the EIS results concerning the activation losses is done with Tafel plots. Different gas diffusion media was used to verify the effect of mass transfer.

Chapter 6 describes the validation of the equivalent circuit model. The equivalent circuit model is used to characterise different types of MEAs in a PEM electrolyser. A comparison of the performance of the different MEAs is shown. The optimal operating current densities is determined from the EIS results.

In chapter 7 conclusions are made regarding the characterisation of the PEM electrolyser. The advantages of using the EIS method are discussed and recommendations for future work on characterising PEM electrolysers are made.

CHAPTER 2

LITERATURE STUDY

2.1 Introduction

The fundamentals of PEM electrolysers are the main focus of this chapter. The electrochemical process of a PEM electrolyser is discussed. A short introduction to the theoretical models based on the Nernst and Butler-Volmer equations are presented. Equivalent circuit model components which form part of the characterisation process are discussed. Three different electrochemical characterisation methods are mentioned. Previous work on PEM electrolyser analysis and approaches followed by previous researchers to characterise PEM fuel cells and electrolysers are considered. A critical overview of the literature is given at the end of the chapter.

2.2 Basic electrolyser operation

A basic schematic of an electrolyser is shown in figure 2.1. The electrolyser consists of a proton exchange membrane, the anode and the cathode. The electro-catalytic layers are situated between the anode (cathode) and the membrane and form the anode (cathode) electrode. When these electrodes are bonded to the membrane, it is called the

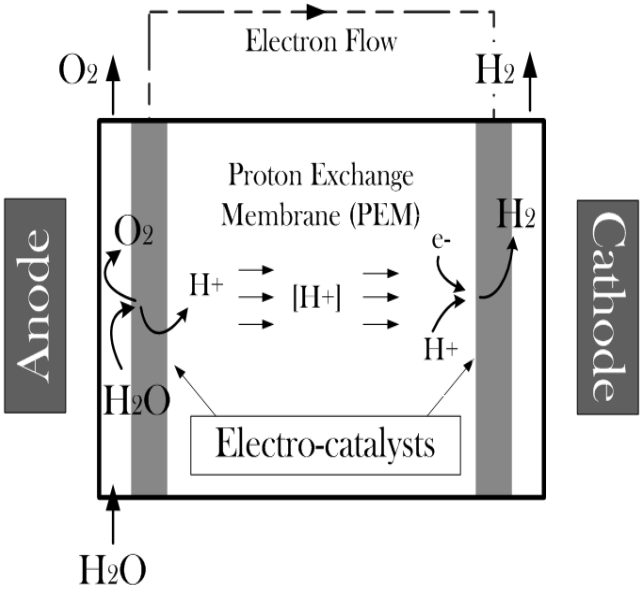

Figure 2.1: Electrolyser schematic [3]

membrane electrode assembly (MEA).

The electrolysis of water is a process where water is decomposed and hydrogen is produced. The first reaction at the anode is given by (2.1). Water is decomposed into oxygen and hydrogen protons as seen at the anode side in figure 2.1. The oxygen produced is separated and vented in the atmosphere. Equation (2.2) represent the reaction at the cathode. At the cathode side in figure 2.1 the positive hydrogen protons and electrons recombine to form hydrogen gas. The overall reaction is shown in (2.3).

$$2H_2O \rightarrow 4H^+ + O_2 + 4e^- \tag{2.1}$$

$$4H^+ + 4e^- \rightarrow 2H_2 \tag{2.2}$$

$$2H_2O \rightarrow 2H_2 + O_2 \tag{2.3}$$

When water is supplied to the anode, hydrogen ions and electrons form as described in (2.1). The protons travel through the proton conductive membrane to the cathode side. The electrons cannot travel through the membrane and exit the cell via the external power supply. The external power supply supplies the potential that drives the reaction. The protons and the electrons reach the cathode and reacts to form hydrogen as shown in (2.2).

2.3 PEM electrolyser models

2.3.1 Theoretical models

Theoretical models are important for fundamental knowledge of a PEM electrolyser. The Gibbs free energy, Nernst and Butler-Volmer are models that describe the electrochemical reactions in a PEM electrolyser. These models are briefly discussed in this section. The full details of these models are discussed in Appendix A.

Gibbs free energy

Josiah Willard Gibbs defined the Gibbs free energy in 1873 [13]. This thermodynamic property predicts that a process will occur spontaneously at a constant temperature and pressure. The Gibbs free energy describes the maximum amount of work that can be performed as a result of the chemical reaction [14].

The Gibbs free energy can be written as

$$\Delta G = \Delta G^0 + RT \ln \frac{[R]}{[O]}, \tag{2.4}$$

where ΔG^0 is the standard free energy, $[R]$ is the activity of the product and $[O]$ is the activity of the reactant at equilibrium. R is the ideal gas constant and T is the temperature in Kelvin [15]. ΔG is the energy available in a system at constant pressure and constant temperature. The Gibbs free energy equation is used to derive the Nernst equation.

Nernst equation

The Gibbs free energy only provides information about a chemical reaction but the PEM electrolyser consist of electrochemical reactions. The Nernst equation adds a another characteristic, electrical energy to the Gibbs free energy. The thermodynamic electrode potential is calculated by the Nernst equation.

Using (2.1) and (2.2) the electrode potential at the anode is given by

$$E_a = E_a^0 + \frac{RT}{2F} \ln \frac{[H^+]^4}{P_{O_2}}, \tag{2.5}$$

and the electrode potential at the cathode is

$$E_c = E_c^0 - \frac{RT}{4F} \ln \frac{[H_2]}{P_{H_2}[H^+]^4}. \tag{2.6}$$

P_{O_2} and P_{H_2} are the partial pressures of oxygen and hydrogen gases. At the cathode the potential is dependent on water as a liquid. The activity of water is usually considered to be one [16]. The full derivative of the Nernst equation is given in Appendix A.

Bulter-Volmer

The Nernst equation is useful to calculate the electrode potential but gives no information about the reaction rate. The link between the reaction rate and electrode potential is done by the Butler-Volmer equation.

The forward reaction rate for the electrochemical reaction is

$$i_f = i_0 \exp(-\frac{\alpha F \eta}{RT}), \tag{2.7}$$

and the backward reaction rate is

$$i_b = i_0 \exp\left[\frac{(1-\alpha)F\eta}{RT}\right], \tag{2.8}$$

where i_f and i_b are the forward and backward current density, i_0 is the exchange current density and η is the overpotential [17]. α is the symmetry factor which is usually 0.5. The rate of the total reaction is the backward reaction subtracted from the forward reaction:

$$i = i_f - i_b = i_0 \left[\exp(-\frac{\alpha F \eta}{RT}) - \exp(-\frac{(1-\alpha)F\eta}{RT})\right]. \tag{2.9}$$

2.3.2 Equivalent circuit models

The electrolyser is an electrochemical system with reactions at the electrodes and at the electrode/membrane interface. These reactions consist of membrane resistance,

charge transfer at the electrode interface and mass transport [3]. Each process can be presented by an electrical circuit element. The whole electrolyser can be represented by an equivalent electric circuit containing resistances, capacitors, inductors or special dedicated elements in parallel or series.

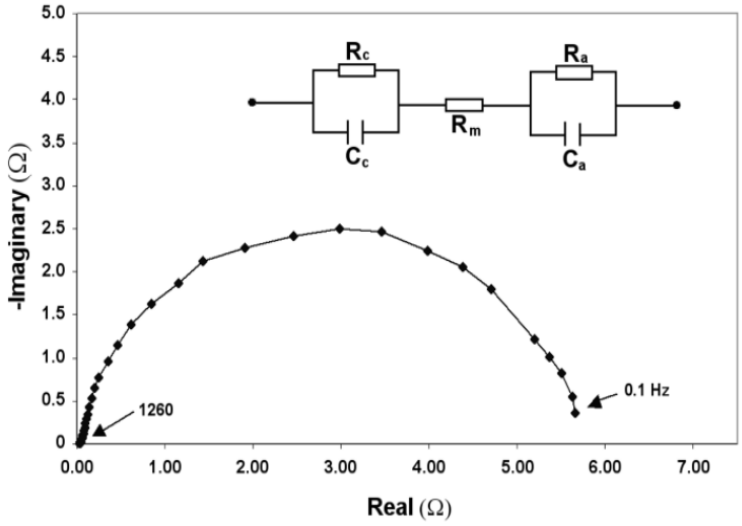

Figure 2.2: Nyquist plot and equivalent circuit model

Figure 2.2 shows a Nyquist plot of a proton exchange membrane fuel cell (PEMFC) and the equivalent circuit model. The experimental EIS data is fitted to the equivalent circuit model. At high frequencies the imaginary impedance is zero which results in a pure resistance equal to R_m, the membrane resistance. At low frequencies the resistance is the sum of R_m, R_a and R_c, from which the charge transfer resistance can be calculated. The maximum imaginary impedance is equal to $R_c R_a C_c C_a$. The detail of the technique is discussed in the next chapter.

2.4 Electrochemical characterisation methods

2.4.1 Polarisation curve

A plot of cell voltage against current density is known as a polarisation curve. The polarisation curve is the standard electrochemical technique to characterise the

performance of electrochemical cells [18]. The polarisation curve for a single cell electrolyser has three regions as shown in figure 2.3. The activation polarisation region is at low current densities. The intermediate current densities is called the ohmic polarisation. This is due to the resistance of the flow of ions through the membrane [12]. The high current density region is called the concentration polarisation. Mass transfer effects dominate this region.

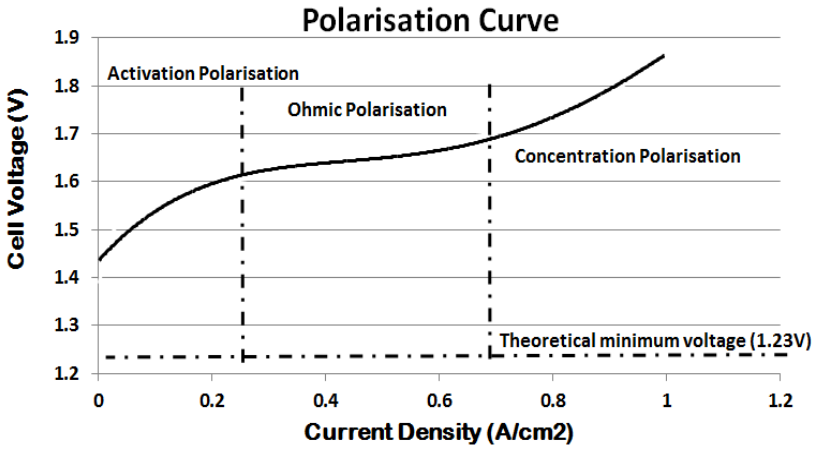

Figure 2.3: Typical PEM electrolyser polarisation curve

Polarisation curves are useful to indicate the overall performance of a cell. Polarisation curves cannot be executed during normal operation and can be time consuming. This technique cannot give any information about the individual components within the electrolyser cell [19].

Tafel slope

In 1905, Julius Tafel found the relationship between overpotential and current density. A plot of log i versus η is known as a Tafel plot. This is useful to evaluate the kinetic parameters. In general there is an anodic branch with a slope of $(1-\alpha)F/2.3RT$ and a cathodic branch slope of $-\alpha F/2.3RT$. As shown in figure 2.4 both linear slopes extrapolate to an intercept of log i_0. As η approaches zero the plot deviates from the linear behaviour because the back reactions can no longer be neglected.

Without much difficulty the transfer coefficient, α and the exchange current density, i_0

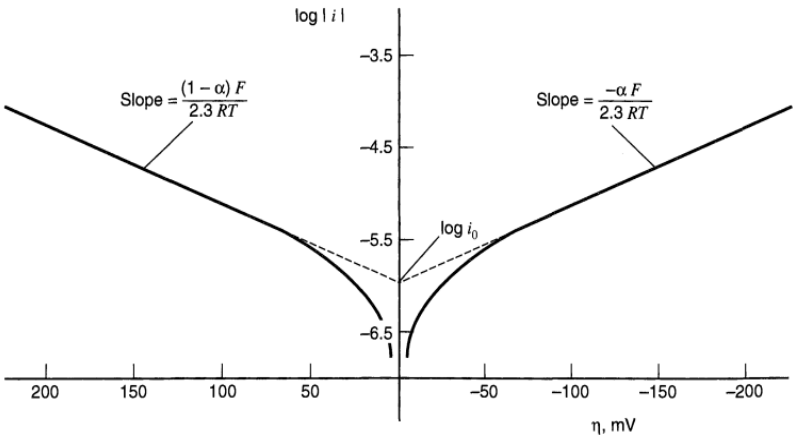

Figure 2.4: Tafel plot for current-overpotential curve [4]

can be calculated.

2.4.2 Current interrupt

The current interruption method is used to measure the membrane resistance of an electrochemical cell. The principle of the technique is that the membrane resistance vanishes faster than the potentials at the electrode when the current is removed [20].

The current interruption technique is useful to determine the ohmic and activation losses. The analysis of the data is relatively easy. The recording of the data should be fast and a high bandwidth oscilloscope is needed to perform this method [12].

2.4.3 Electrochemical impedance spectroscopy

Unlike the other methods like the current interruption where the system needs to shut down, EIS applies a small perturbation AC signal to the cell at steady state. A known signal of voltage (or current) is applied to the cell and the resulting signal current (or voltage) is measured as a function of frequency. The impedance can be measured over a wide range of frequencies.

The range of impedance is shown in a Nyquist plot. The behaviour of the electrodes, membrane and the electrode-membrane interfaces can be determined. The advantage

of EIS is the ability to resolve, in the frequency domain, the various losses associated with a PEM electrolyser [21]. The losses includes the ohmic, activation and mass transfer losses.

2.5 Literature review

The principles of PEM fuel cells and PEM electrolysers are basically the same. The only difference is that the chemical reaction works in the opposite direction. Some of the research done on fuel cells can be applied to electrolysers. Although the focuses of the research is done on the PEM fuel cells, a couple of researchers have studied the PEM electrolyser. The following literature focus on recent advances on PEM electrolysers and fuel cells.

2.5.1 Operating conditions

The operating conditions are critical aspects of a PEM electrolyser. The flow rate of the water supply is crucial to prevent flooding or drying of the membrane. Temperature and pressure have an effect on the performance of the electrolyser.

Costamagna [22] studied critical operating conditions such as flooding, membrane drying and degradation due to temperature peaks. A simulation model based on transport and balance equations was developed to evaluate the chemical parameters. Mass, energy, momentum and electrical transport phenomena in a PEM fuel cell were investigated.

Mrida et al. [23] also studied two failure modes, flooding and dehydration of a four-cell PEM fuel cell. EIS was used to investigate these two modes. In the study a fuel cell was operated at 70 and 80 °C, the current density varied from $0.1 - 1.0$ A/cm^{-2} and the EIS test frequency was between 0.1 Hz and 200 kHz. The effect of dehydration was observed from 0.5 Hz to 100 kHz. The flooding effect could only be seen from 0.5 Hz to 100 Hz. They proposed that impedance spectroscopy can be used to differentiate

between dehydration and flooding of the PEM fuel cell using narrow frequency bands for dehydration and flooding.

2.5.2 Proton exchange membrane

The proton exchange membrane is responsible for the principle on which electrolysers and fuel cells work. The properties of the membrane play an important role in the performance of the electrolyser.

Freire and Gonzlez [24] studied an H_2/O_2 single cell polymer electrolyte fuel cell with four different Nafion® membranes. The effect of temperature, membrane thickness and humidification conditions were investigated using an impedance response technique. The high frequency resistance, low frequency relaxation and the oxygen reduction reaction (ORR) were part of the impedance analyses. They determined that the low frequency relaxation process is mainly due the flooding of the cathode with liquid water and limited solvability of oxygen in water for the oxygen reduction reaction. They concluded that thinner membranes are less sensitive for temperature and current density changes.

Andreaus et al. [25] also compared the impedance with different membranes only varying the thickness of the membranes. It was concluded that an increase in the high frequency impedance resistive component with an increase in the thickness of the membranes. The fuel cell was operated at high current densities.

2.5.3 Electro-catalyst

The electro-catalysts on the anode and cathode side are critical elements. The activity of the cell is proportional to the performance of the electro-catalyst which primarily consists of noble metals (Pt, Ir or Ru).

Song et al. [26] studied the electrode of a PEM fuel cell to find the optimal composition of the electrodes using impedance spectroscopy methods. They placed a thin catalyst-supporting layer between the gas diffusion layer and the catalyst layer.

The catalyst layer was cast on top of this supporting layer. The proper solution ratio for ionomer Nafion and Pt/C catalyst was optimised to 0.8 mg/cm^{-2} and 0.4 mg/cm^{-2} respectively.

Eikerling et al. [27] used a macro-homogeneous model to calculate the small-signal dynamic response of the cathode catalyst layer. This approach included the reaction kinetics and the double layer capacitance at the catalyst/electrolyte interface. A correlation between the impedance spectra and analytical derived expressions was made. The separation between the catalyst layer contribution and the other fuel cell components was given.

Marshall et al. [28] mentioned that water electrolysis has many advantages over traditional technologies which include higher energy efficiencies, a high production rate and a compact design. They also stated that the anode has the largest over-potential when operated at typical operating current densities. They suggested that by developing a better electro-catalyst for the oxygen evolving electrode, better efficiencies can be reached. They used cyclic voltammetry and steady state polarisation analysis to distinguish between the effects of the electro-catalytic activity and active surface area. Understanding these two factors are critical for developing a better electro-catalytic material to improve the performance of a PEM electrolyser. Overall the best cell voltage obtained was 1.567 V at 1 A/cm^{-2} when Nafion 155 was used at 80 °C.

2.5.4 Modelling

Obtaining a model for an electrochemical system containing electrical and chemical processes is a challenging task. The model should be able to represent the behaviour of the electrolyser. Different model types are proposed in the following literature.

Choi et al. [29] developed a simple but useful basic theoretic model. The model is based on the Butler-Volmer kinetics for a polymer electrolyte. The relation between the applied voltage and the current density is expressed in terms of the Nernst

potential, exchange current densities and the resistance of the electrolyte. The over-potentials and resistances at the anode and cathode are analysed and correlate with the experimental results. They concluded that the oxidation at the anode creates the largest over-potential.

Marangio et al. [30] analysed the performance of a high pressure PEM electrolyser using an equivalent circuit model. The theoretical open-circuit voltage is calculated via thermodynamic analysis which forms part of the proposed model. The model predicts the expected real voltage during operation by calculating the different over-potentials in terms of the current density. A polarisation curve of the model is compared with the experimental data and some important process parameters and their trend in different conditions are obtained.

H. Görgün [31] described a dynamic model for a PEM electrolyser based on the mole balance between the anode and cathode. The model is also based on water phenomena, electro osmotic drag and diffusion in the membrane. It is designed for a control strategy that will ensure that the electrolyser is safely operated at high efficiencies.

2.5.5 PEM electrolysers versus alkaline electrolysers

PEM electrolysers have a number of advantages over the water alkaline electrolyser, which include ecological cleanliness, smaller mass-volume characteristics, electricity costs, high purity of hydrogen production and the opportunity of compressed gasses within the cell [3]. The high cost of the membrane, electro-catalyst with noble metal (Pt, Ir, Ru) and the requirements of clean water result in a rather high cost of this type of electrolyser. Although the capital cost of alkaline electrolyser is lower, 70% of the cost of alkaline electrolysers usually consists of electricity costs.

2.6 Critical overview

Throughout this chapter the characterisation of a PEM electrolyser is confronted with intricate electrochemical processes. The purpose of this section is to critically evaluate the solutions found in the literature, in the context of characterising a PEM electrolyser.

Theoretical models such as the Nernst and Butler-Volmer models can calculate the theoretical cell potential. There exists a gap between the theoretical potential and the actual potential. The difference between these values is called the overpotential. The overpotentials can be interpreted as losses. The theoretical models cannot calculate these overpotentials and therefore equivalent circuit models are used.

Electrochemical characterisation methods include the polarisation curve, current interrupt and EIS. The polarisation curve is a standard method to evaluate the performance of the electrolyser. The polarisation curve data does not give information about the individual components and cannot be used in an equivalent circuit model.

The current interrupt method is used to measure the membrane resistance with the possibility to identify the charge transfer resistances. The current interrupt method is currently being studied in another project at HySA Infrastructure and is not part of this study.

The EIS method has the ability to distinguish between the processes in the PEM electrolyser [32, 33]. The ohmic and charge transfer resistances can be determined by EIS. The mass transfer effect can limit the performance of the PEM electrolyser and EIS can also identify this effect. The method is used when the electrolyser is operated at steady state conditions. The EIS method can determine the ohmic, activation and mass transfer overpotentials/losses. These are the main losses in a PEM electrolyser. By identifying these losses the electrolyser can be characterised. Thus EIS is the preferred method and the focus of the next chapter.

CHAPTER 3

ELECTROCHEMICAL IMPEDANCE SPECTROSCOPY

3.1 Introduction

The literature study in chapter 2 highlighted an electrochemical technique, EIS, which can be used to characterise PEM electrolysers. Therefore this chapter will focus on electrochemical impedance spectroscopy as an electrochemical method. The origin of EIS is discussed as well as the principles on which the technique is based. The data collected is illustrated using Nyquist plots. Circuits and circuit elements that are often used to describe the PEM electrolyser are discussed. The important effect of circuit ambiguities is mentioned.

3.2 Background

Electrochemical impedance spectroscopy is well known in the electrochemical field as an in-situ as well as ex-situ method. The introduction of fuel cells in the late 1950's, linked electrochemists and material scientists. The focus of analyses shifted from the time domain to a frequency domain, towards a small perturbation signal.

Techniques such as current interruption, cyclic voltammetry, potential sweeping

and EIS have been used to investigate different aspects of the electrolyser. The polarisation curve characteristics are useful to identify important electrochemical parameters such as exchange current densities, Tafel slopes and diffusion coefficients. Polarisation curves provide only important data of the performance of the electrolyser. Unfortunately polarisation curves provide no information about the membrane-electrode interface mechanisms and the individual contribution of each process occurring at the electrode level. Current interruption on the other hand is a method used only to measure the ohmic resistance of a membrane. EIS is a technique frequently applied and recently it is known as a primary tool in fuel cell research [21].

One of the most attractive aspects of impedance spectroscopy as a tool for investigating the electrical and electrochemical properties of materials and systems, is the direct connection that often exists between the behaviour of a real system and that of an idealised circuit model consisting of electrical components. The investigator typically compares or fits the impedance data to an equivalent circuit model, which is a representation of the physical processes taking place in the system under investigation.

3.3 Principle of EIS

A small perturbation of AC current is applied while the electrolyser is operating at steady state conditions as depicted in figure 3.1. There are three different types of electrical perturbations which are used in the electrochemical field:

First, in the transient measurements a step function ($V(t) = V_0$ for $t > 0$, $V(t) = 0$, for $t < 0$) is applied at $t = 0$ to the system. The corresponding time- varying current $i(t)$ is measured. The relationship $V_0/I(t)$ is called the time varying resistance. The advantage of this method is that it is experimentally easily accomplished. The disadvantage is that the results must be transformed with the Fourier or Laplace-transform and the signal-to-noise ratio varies at different frequencies. This method is easy to formulate but not often used in EIS.

The second method is to compose the stimuli voltage $v(t)$ with random (white) noise.

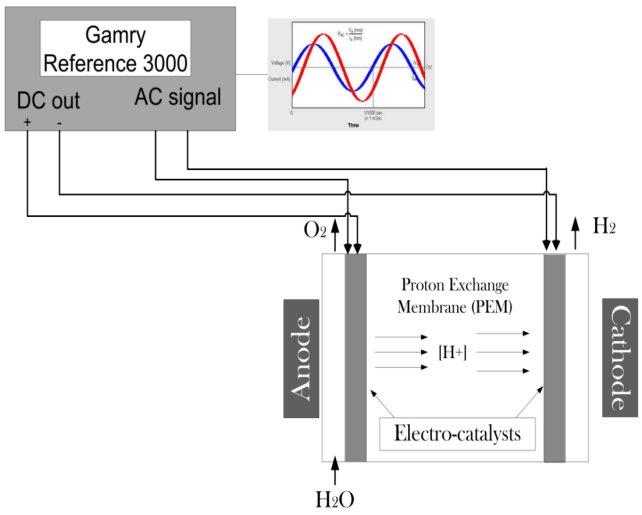

Figure 3.1: Applying a small AC perturbation signal

The corresponding current $i(t)$ is also measured and the result will pass through one general Fourier-transform. The advantage of this method is fast data collection but the disadvantage is the production of true white noise. A sum of different sine waves can be applied to optimise the signal-to-noise ratio.

The third method is defined by applying a single-frequency voltage or current and to measure the resulting current or voltage as depicted in figure 3.2. The phase shift θ is calculated to measure the impedance. Electrochemical equipment is available which measure the impedance as a function of frequency automatically. This method is most commonly used in the electrochemical environment [33].

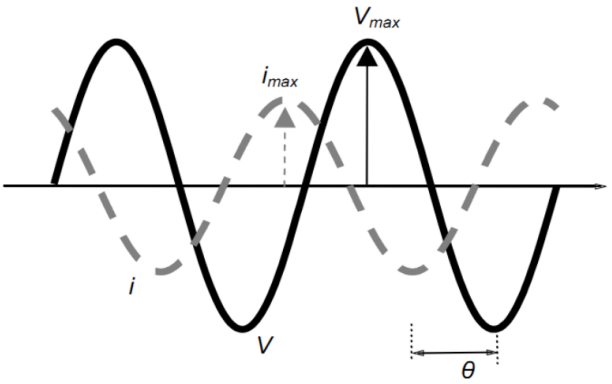

Figure 3.2: The applied and response waveforms of the EIS technique

The frequency of the AC current is swept and the corresponding AC voltage of each

frequency step along with the phase angle is measured. The data is used to calculate the real and imaginary impedances. An example of the relationship between the voltage and the current is shown in figure 3.2. The real part of the impedance is associated with pure resistance and the imaginary part is associated with inductance and capacitance.

3.3.1 Response to a small-signal perturbation in the time domain

A voltage $v(t) = V_{max}\sin(\omega t)$ containing a single frequency $f \equiv \omega/2\pi$ is applied to the cell. A current $i(t) = I_{max}\sin(\omega t + \theta)$ is measured. The phase difference between the voltage and the current is represented by θ. θ is zero for a purely resistive cell. The response of capacitive and inductive elements in (3.1) and (3.2) involve difficult calculations in the time domain.

$$i(t) = C\left[\frac{dv(t)}{dt}\right] \tag{3.1}$$

$$v(t) = L\left[\frac{di(t)}{dt}\right] \tag{3.2}$$

3.3.2 Response to a small-signal perturbation in the frequency domain

The Fourier transformation is used to simplify the calculations by converting the equations to the frequency domain. Equations (3.1) and (3.2) can be transformed to (3.3) and (3.4). Note that $j \equiv \sqrt{-1}$, then

$$I(j\omega) = Cj\omega V(j\omega), \tag{3.3}$$

$$I(j\omega) = \frac{V(j\omega)}{(Lj\omega)}. \tag{3.4}$$

In the frequency domain the voltage and the current are written in a Ohm's law form,

$$I(j\omega) = \frac{V(j\omega)}{Z(j\omega)}, \tag{3.5}$$

where the complex capacitance is

$$Z_C(j\omega) = \frac{1}{(j\omega C)}, \tag{3.6}$$

and the complex inductance

$$Z_L(j\omega) = j\omega L. \tag{3.7}$$

The value of $Z(j\omega)$ at any specific frequency is the impedance of the electric circuit. In the frequency domain, Ohm's law is used and simplifies the calculations.

The concept of complex impedance is expressed by a vector sum of components x and y along the axis, that is $Z = x + jy$. The imaginary number $j \equiv \sqrt{-1} \equiv e^{j\pi/2}$ indicates a rotation of $\pi/2$. The real part of Z is in the direction of the x axis and the imaginary part of Z is in the y axis direction as shown in figure 3.3.

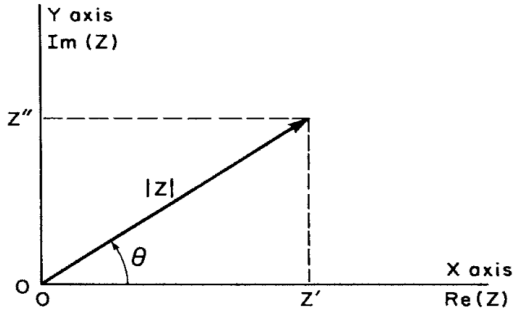

Figure 3.3: The real and imaginary parts of impedance

The impedance

$$Z(\omega) = Z' + jZ'', \tag{3.8}$$

where Z' is the impedance along the real axis. Z'' is the impedance along the imaginary axis. The real part of the impedance can be calculated by

$$\mathrm{Re}(Z) \equiv Z' = |Z|\cos(\theta), \tag{3.9}$$

and the imaginary part of the impedance by

$$\mathrm{Im}(Z) \equiv Z'' = |Z|\sin(\theta). \tag{3.10}$$

The phase angle

$$\theta = \tan^{-1}(\frac{Z''}{Z'}), \tag{3.11}$$

and the modulus is

$$|Z| = [(Z')^2 + (Z'')^2]^{1/2}. \tag{3.12}$$

The data collected by applying the EIS method can be illustrated with a Nyquist plot. A Nyquist plot is the graphical display of complex numbers where the x-axis represent the real part and the y-axis the imaginary part. The convention is made that the negative imaginary values are placed on the y-axis as shown in figure 3.4. Each point on the plot is the complex impedance at the frequency at which the impedance was measured. Figure 3.4 shows a typical Nyquist plot.

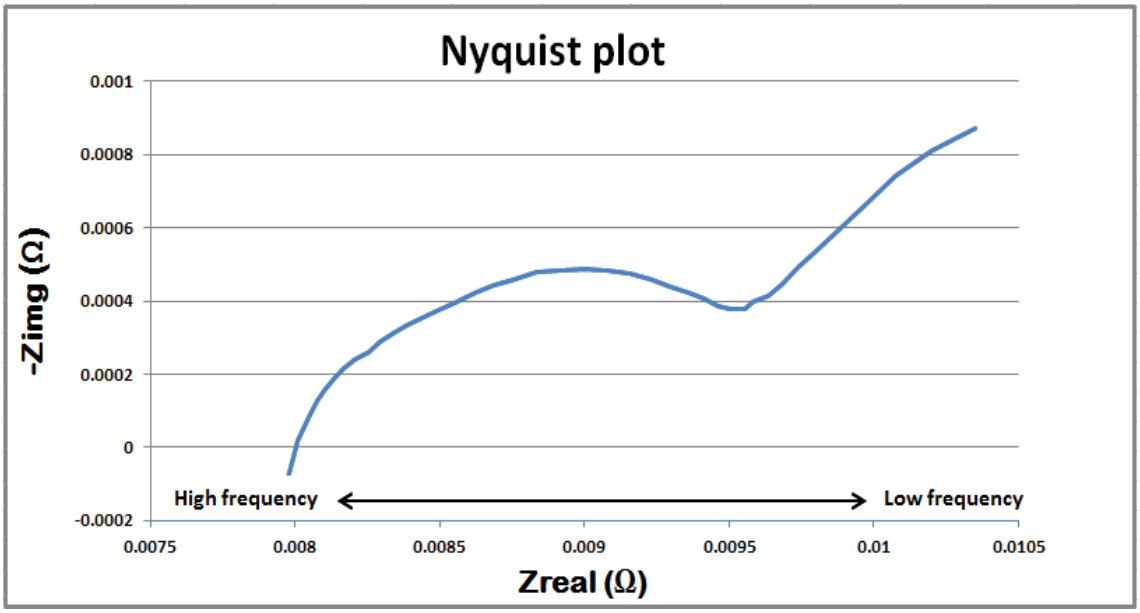

Figure 3.4: Nyquist representation

3.4 Equivalent circuit elements

The response of an electrical circuit can be displayed in a Nyquist plot. The aim is to construct an equivalent circuit model with the same Nyquist plot as the EIS data of the PEM electrolyser. The components of the equivalent circuit model can be used to

describe the processes in the electrolyser. The development of an equivalent circuit model is discussed in chapter 4. The components of the equivalent circuit is the focus of this section. Each possible element will be discussed in the following section.

3.4.1 Resistors

The impedance of a pure resistor is shown in (3.13). ω is the frequency of the perturbation AC signal.

$$Z_R(\omega) = R \tag{3.13}$$

In the frequency domain a resistor has only a real part. The real and the imaginary part of the impedance are $Z_{re} = R$ and $Z_{im} = 0$ respectively.

Three primary types of resistances are investigated for the equivalent circuit modelling of an electrolyser: ohmic, electrolyte and charge transfer resistance.

Electrolyte and ohmic resistance

The electrolyte resistance R_M is the resistance of the membrane when current is passed through the membrane. R_M is proportional to the resistivity ρ of the membrane and the thickness δ of the membrane. The resistance is given by

$$R_M = \rho\delta. \tag{3.14}$$

The conductors and conducting polymers also have a resistance. This resistance is often ignored because it is small compared to the electrolyte resistance. The ohmic resistance is the electrolyte and the resistances associated with the conductors.

Charge transfer resistance

The charge transfer resistance refers to the loss of energy when an electron pass from the electrode surface to the membrane or visa versa. This resistance causes an overpotential. As the overpotential becomes larger the charge resistance diminishes.

3.4.2 Capacitors

The capacitance is represented by the electric charge divided by the voltage drop across the capacitor

$$C = \frac{Q}{V}. \tag{3.15}$$

The impedance of a capacitor is given by

$$Z_c(\omega) = \frac{1}{j\omega C}. \tag{3.16}$$

A pure capacitor has a component along the negative imaginary axis and no component along the real axis.

Double-layer capacitance

An electrical double layer forms at the interface between the electrode and the membrane. This double layer acts as a capacitor and is called the double-layer capacitance. Equation (3.17) shows the double-layer capacitance:

$$C_{dl} = \left[\frac{\partial \sigma_E}{\partial E}\right]_{T,p,\mu}, \tag{3.17}$$

where T is the temperature, p is the pressure and μ is the chemical potential. E is the potential and σ_E is the charge transfer [34].

3.4.3 Distributed elements

In electrochemistry it is often not possible to describe the response of the system with a combination of pure capacitors or resistors. Two distributed elements are used for these model behaviours. There are two distributed elements, the constant phase element (CPE) and the Warburg impedance [35].

Constant phase element

The CPE can be associated with surface roughness, varying thickness or non-uniform current distribution. It was noted that electrochemical systems did not respond as pure capacitors and resistors would and these special elements were derived. A Nyquist plot of a resistor in parallel with a capacitor should be a semicircle with the centre on the x-axis, but it was observed that the semicircle shifted with the centre somewhere below the x-axis. Figure 3.5 shows the shift of the semicircle with a resistor in parallel with a CPE [36].

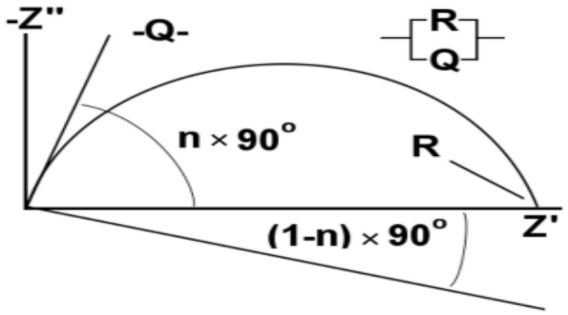

Figure 3.5: Nyquist plot to illustrate the effect of the CPE

The impedance of a CPE is

$$Z_{CPE}(\omega) = q^{-1}(j\omega)^{-n}, \tag{3.18}$$

where n is the factor which indicates the phase shift. The CPE can represent a pure resistor ($n = 0$) or a pure capacitor ($n = 1$). q is a proportional factor with numerical values.

Warburg impedance

The Warburg impedance is related to mass transfer in a electrochemical system. The impedance is written as

$$Z_\omega = \sigma\omega^{-0.5} - j(\sigma\omega^{-0.5}), \tag{3.19}$$

where

$$\sigma = \frac{1}{nFA\sqrt{2}}\left(\frac{\beta_O}{D_O^{0.5}} - \frac{\beta_R}{D_R^{0.5}}\right). \tag{3.20}$$

The Warburg impedance can be identified as a 45° line in a Nyquist plot following the semicircle. This is due to the series connection of a resistor ($R = \sigma\omega^{-0.5}$) and the capacitor ($C = \sigma\omega^{-0.5}$).

3.5 Ambiguities

A problem often experienced in equivalent circuit fitting is that different models can have the same impedance signature. Figure 3.6 illustrates the ambiguity of two models.

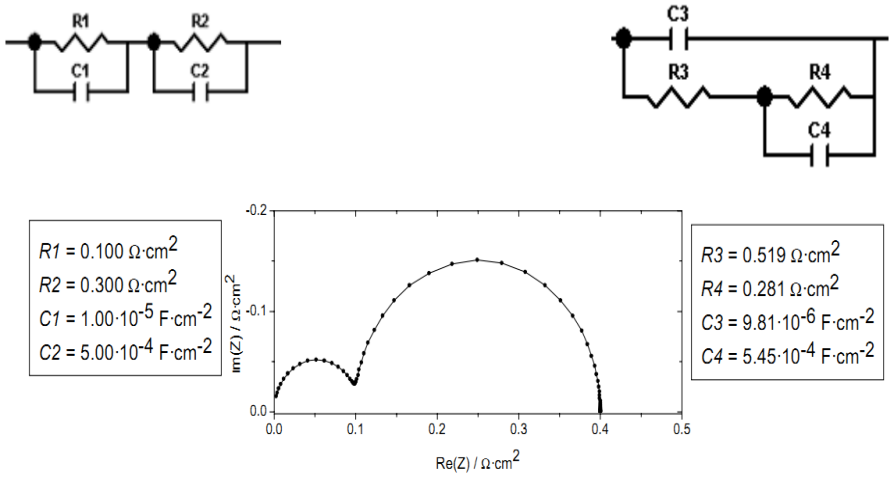

Figure 3.6: Two different models with the same impedance spectrum

The probability that multiple models have the same impedance spectrum can lead to confusion when electrochemical properties are linked to a component. Care should be taken to develop an equivalent circuit model as well as to establish the link between the components and the electrochemical process.

3.6 Conclusion

In this chapter the reader was introduced to electrochemical impedance spectroscopy. The principles of the technique were described as well as an illustration of the response to a small perturbation signal. The Nyquist plots were introduced and some circuit

elements often used in equivalent circuit models and the important role of ambiguities were discussed.

Other techniques like current interrupt and polarisation curve cannot give the same amount of information about the PEM electrolyser as EIS. The current interrupt is an accurate method where only the membrane resistance can be calculated. The polarisation curve only gives the relationship between the current density and the cell voltage. EIS is a method that has the ability to distinguish between the processes in the PEM electrolyser. The three major losses namely ohmic, activation and mass transfer can be identified using EIS.

After identifying EIS as the method to characterise an PEM electrolyser, an equivalent circuit model needs to be developed. The components of the equivalent circuit model are described in this chapter. The next chapter is devoted to develop an equivalent circuit model. The EIS data from the PEM electrolyser will then be used to optimise the parameters in the equivalent circuit model representing the processes in the PEM electrolyser.

CHAPTER 4

CHARACTERISATION PROCEDURE

4.1 Introduction

The PEM electrolyser characterisation procedure includes three important aspects, as shown in figure 1.3 in section 1.4.1. First experimental data of the PEM electrolyser is required. An equivalent circuit model is developed to represent the processes of a PEM electrolyser. The characterisation process is completed by fitting the experimental data to the equivalent circuit model.

The first part of this chapter focuses on the experimental setup and data acquisition. This section provides information about the experimental setup and the hardware that has been used. The data generated when the EIS technique is applied is discussed.

The second part of this chapter focuses on the development of an equivalent circuit model. The purpose is to develop an equivalent circuit with the same frequency response as the experimental data generated using EIS. The iterative procedure for developing an equivalent circuit model is described in this section. This section includes models developed in the literature. The development starts with the basic Randles cell and then the effect of mass transfer is added to the model with the use of the Warburg impedance. Then the CPE is added to increase the accuracy of the model.

The final equivalent circuit model is discussed at the end of the section. The final part of this chapter describes the data fitting method.

4.2 Experimental setup

The experimental setup which is used to obtain the impedance spectra and polarisation curves consists of three main components: the electrolyser test setup, the electrolyser and the EIS equipment. Each component is briefly discussed in the following sections.

4.2.1 Electrolyser test setup

The test bench is at the North-West University in the HySA Infrastructure membrane and electrolysis laboratory. The bench provides the necessary hardware and a safe environment to operate the electrolyser. Figure 4.1 shows the components of the test bench.

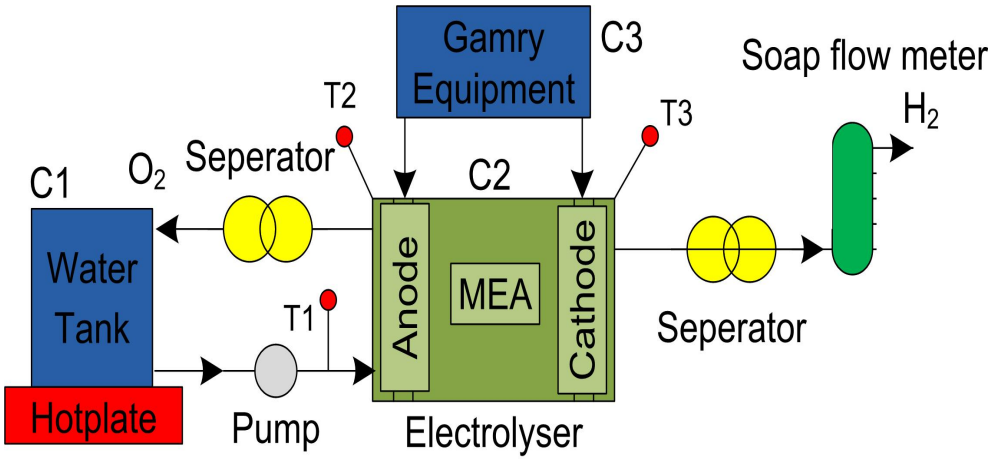

Figure 4.1: Experimental Setup

C1 is a water tank that supplies deionised (DI) water to the cell. The quality of the water is important in any water electrolysis system. The DI water needs minimum resistivity of 1 MΩ [32]. C1 is also used to separate the oxygen produced when the water flows back to the water supply tank from the anode side. A hot plate and stirrer

are used to heat the water to the desired temperature. A peristaltic pump is used to control the flow rate of the water. The electrolyser, C2 includes the anode, cathode and MEA. Heating pads are used to control the temperature in the electrolyser. T1, T2 and T3 are temperature probes at the inlet, anode and cathode respectively. The electrochemical equipment is present at C3. At the cathode side hydrogen is produced. Water diffuses through the membrane to the cathode side with osmotic drag and needs to be separated. The hydrogen production rate is measured with a soap flow meter. Figure 4.2 shows the setup in the laboratory.

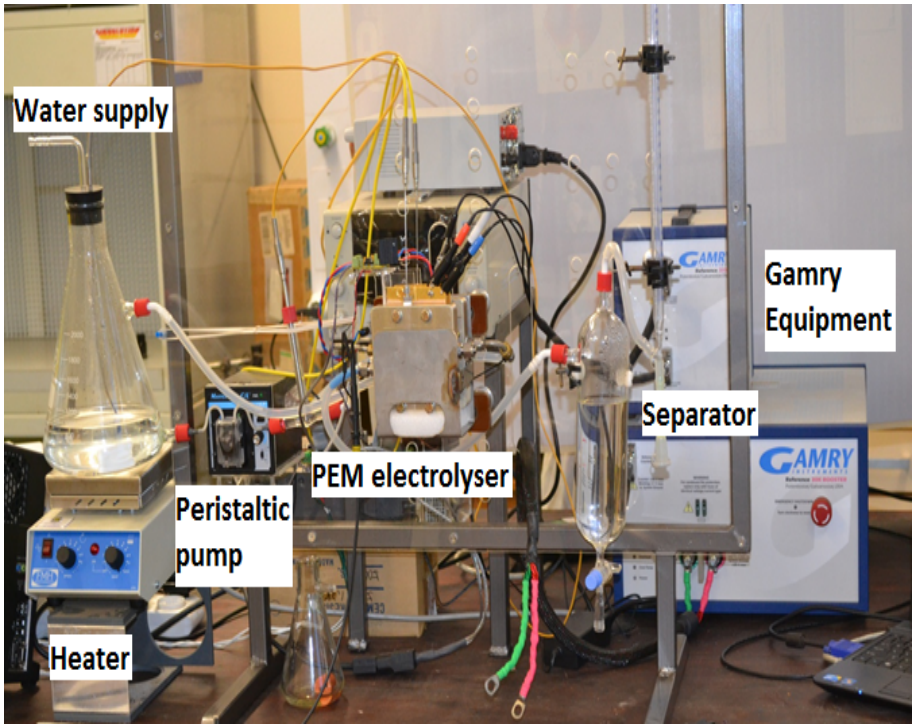

Figure 4.2: Laboratory setup

4.2.2 The electrolyser

The electrolyser cell in figure 4.3 is used in all the experiments. It is supplied by Fuel Cell Technologies, Inc. and a conversion kit from Proton Onsite is used to convert the fuel cell to an electrolyser. The conversion kit replaces the graphite flow field with a titanium flow field. This material was preferred due to its high corrosion resilience for the oxygen evolution reaction (OER).

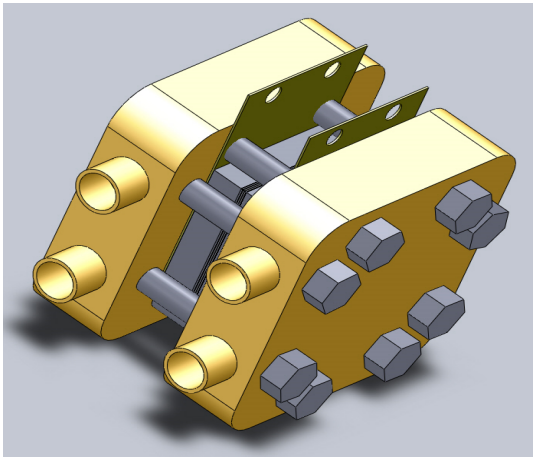

Figure 4.3: CAD representation of the electrolyser

The single cell electrolyser is composed of two current collector plates and two flow field plates with an MEA between them sealed with gaskets. Figure 4.4 shows the assembly of the electrolyser.

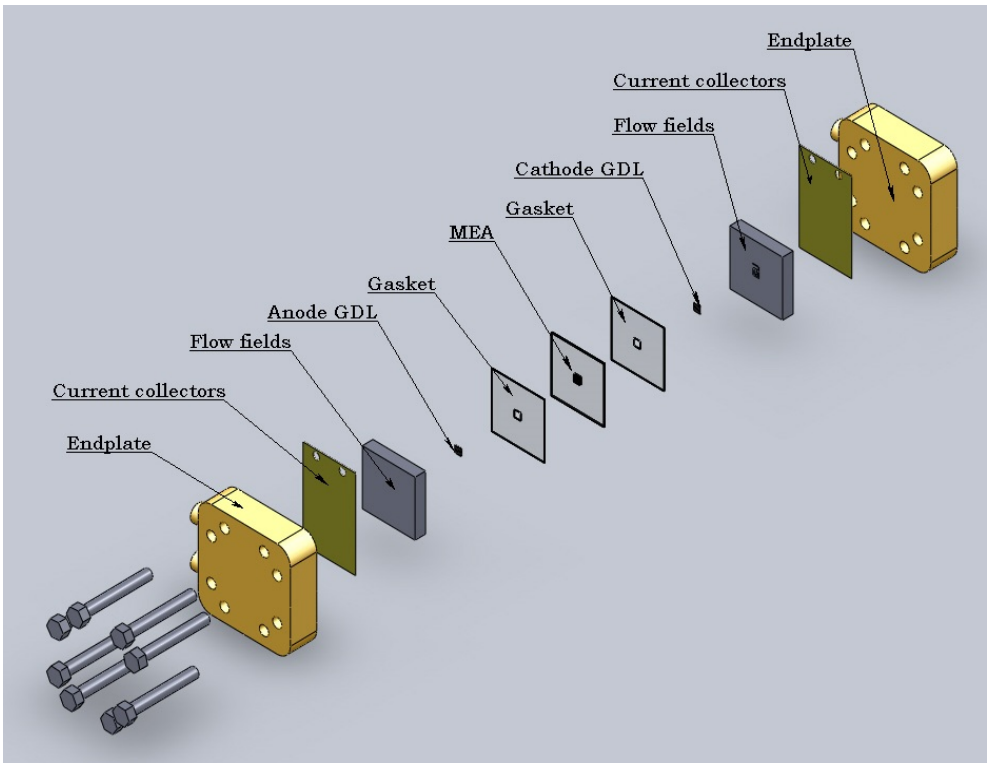

Figure 4.4: Assembly of the electrolyser

Two end-plates are used primarily for structural strength. The water supply is connected to the end-plates. Heating pads are situated in the end-plates to heat

the water inside the electrolyser. The water is guided through the end-plates to the flow fields where it is consumed and then guided back to the end-plates and out of the electrolyser. Temperature probes are connected in the end-plates to measure the temperature of the electrolyser. The current collector plates are isolated from the end-plates. The power supply is connected to the current collector plates which are made of gold plated copper.

The flow field in figure 4.5 is specially designed to supply the reactants to the gas diffusion layer (GDL) and MEA and to transport the products away from the GDL and MEA. The products need to be transported away fast enough to make way for the reactants ensuring that no mass transfer occurs.

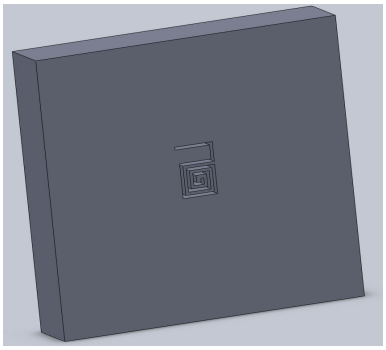

Figure 4.5: Flow field

The GDLs play the role of facilitating gas transport at the electrodes. The GDLs have attracted little attention because of the negligible small effect of mass transfer compared to the catalyst layers. The conductivity of the GDLs is much higher than the conductivity of the membrane.

The MEA is the anode catalyst, membrane and cathode catalyst combined. The anode electro-catalyst plays the most significant role in the electrolyser while the cathode electro-catalyst activity is often neglected. The electro-catalyst usually consists of PtB and IrRuOx. The membranes often used are Nafion® 115, 117 and 1110. The MEA is sealed with a gasket on each side.

4.2.3 EIS equipment

The Gamry Reference 300 is a precision electrochemical instrument. A current booster, 30k Booster from Gamry Instruments, provides the desired current to the electrolyser. Figure 4.6 describes the connection of the Gamry reference 3000 to the PEM electrolyser.

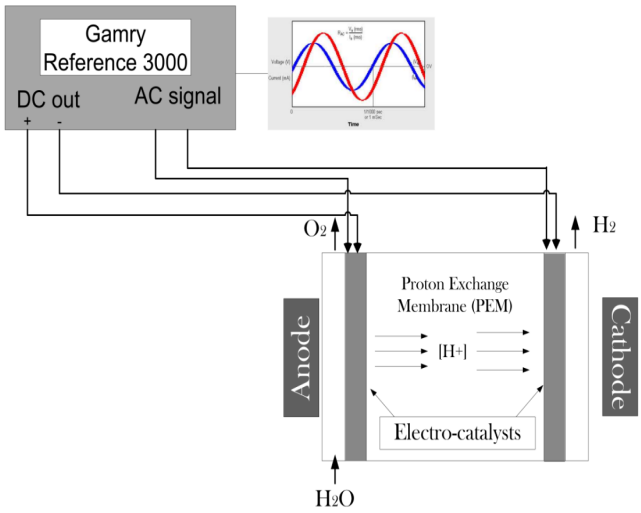

Figure 4.6: Connecting the Gamry to the PEM electrolyser

The electrolyser is connected to the DC power supply of the Gamry and operated at steady state conditions. A small AC signal is added to the DC current which is applied to the electrolyser. The amplitude of the AC signal is 10 % of the DC value. A frequency range is typically between 100 mHz and 200 kHz. The corresponding AC signal is measured to calculate the impedance at the specific frequency.

Table 4.1 summarises the performance of the Reference 3000 and the 30K Booster:

Table 4.1: Gamry equipment specifications

Gamry Reference 300	
Modes	Potentiostat, galvanostat, ZRA, FRA
Cell connections	2, 3 or 4 electrode
Current range	3 A
Current resolution	100 aA

Continued on next page

Table 4.1: Gamry equipment specifications

Voltage range	15 V
Voltage resolution	1 uV
EIS measurement	
	Waveform Sine
	Frequency range 10 uHz - 1 Mhz
	Max Amplitude 1.425 V
	Min Amplitude 2.75 μV
	Weight 7 kg
Gamry 30K Booster	
Compliance Voltage	20 V, -2.5 V
Output current	30 A
Accuracy	0.3mA
Frequency range	200 kHz
Weight	16 kg
Software	PWR800 EIS 300 Software, OptiEIS
PC Interface	USB

The Gamry equipment is calibrated using a calibration board. The equipment is connected to a dummy cell in a Faraday cage to ensure the equipment is calibrated correctly.

4.2.4 EIS data

Electrochemical impedance spectroscopy is a sophisticated technique. The data generated needs to be interpreted to be able to distinguish between the different components of the electrolyser [37].

A small AC current is applied while the electrolyser is operated at steady state

conditions, as discussed in chapter 3, the resulting AC voltage is measured as a function of frequency. The complex impedance as a function of frequency is plotted on a Nyquist plot. A typical interpreted Nyquist plot is shown in figure 4.7.

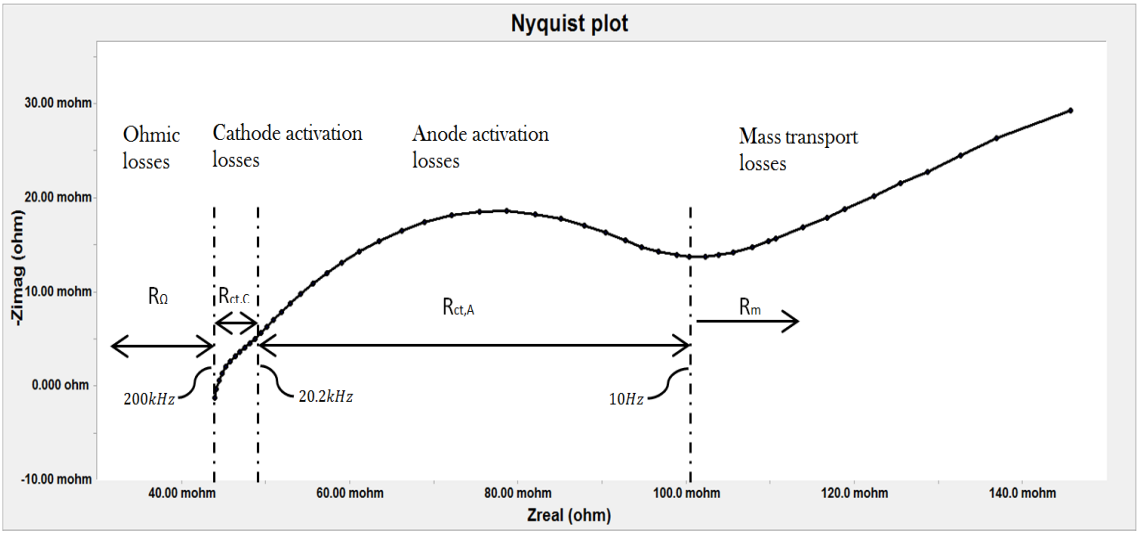

Figure 4.7: Typical Nyquist Plot

In a Nyquist plot the imaginary impedance is plotted against the real part at each frequency ranging from high to low frequency. High frequency is shown at the left of the Nyquist plot and the low frequency is towards the right. The high frequency semicircle reflects the activation resistance while the low frequency data always reflects the mass transport limitations [12].

High frequency arc

The high frequency arc ranges from 200 kHz to 10 Hz. The intercept of the high frequency arc with the real axis indicates the ohmic resistance. This is due to pure resistance which does not have an imaginary part. Ohmic resistance is related to the resistance in the membrane and the conductors (see section 3.4.1).

The hydrogen evolution reaction (HER) takes place at the cathode. This reaction is faster than the oxygen evolution reaction (OER) which takes place at the anode. The impedance spectrum of the electrolyser is almost equal to only the anode impedance. Many researchers use the impedance data of the anode only, since the cathode

impedance is negligible. If the kinetics of the HER is visible, two overlapping semicircles are noticeable in the high frequencies. The smaller semicircle is due to the cathode activation resistance. The second semicircle is the anode activation resistance. The diameter of the two semicircles represent the activation losses which includes the membrane, GDL, bipolar plate and contact resistances. A change in this value during different current densities is related to be membrane hydration and kinetics of the reactions at the anode and cathode [12, 38].

Low frequency

The low frequency region of a Nyquist plot can differ extremely depending on the operating current density. Figure 4.8 shows the Nyquist plot of two different current densities.

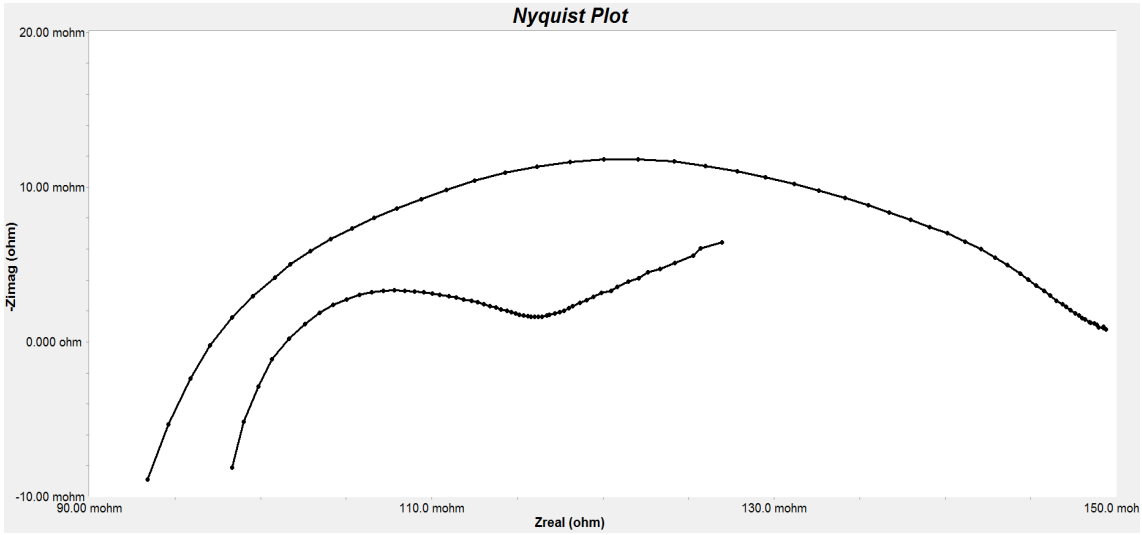

Figure 4.8: Nyquist plot of the same MEA at two different current densities (0.2A/cm^2 and 1A/cm^2)

The most simplified behaviour of the impedance spectrum is a single impedance semicircle. In figure 4.8 the 0.2 A/cm^2 semicircle is a single impedance semicircle. The 1 A/cm^2 impedance spectra shows a 45 $^\circ$ line at low frequencies or the impedance can have a second semicircle (not shown). Wagner et al. [35] identified these phenomena: If no diffusion is present only one arc is present, if diffusion is present and if it is finite,

two arcs are present and if the diffusion is infinite a 45 ° straight line is present at the low frequency region. The impedance spectra at low frequencies always reflects the impedance due to mass transport limitations [12, 39].

4.3 Model development

An equivalent circuit model needs to be developed to characterise the PEM electrolyser by identifying the electrochemical processes. Models found in the literature is used as a mould for the development process. The development of the equivalent circuit model started with the Randles cell. The effect of the diffusion and mass transfer is addressed by adding the CPE and Warburg components discussed in chapter 3. This section illustrates the development process from the Randles cell to the desired equivalent circuit model.

4.3.1 Models from literature

The development of an equivalent circuit model involves an intuitive design process because of the link that has to be established between the circuit parameters and the electrochemical process. Consequently an obvious starting point is looking at resent work done on similar equivalent circuit models in the literature.

Basic model

Andreas et al. [25, 40] investigated performance losses in a polymer electrolyte fuel cell at high current densities. The dependence of membrane thickness was under discussion. Nafion membranes with different thickness and equivalent weights (EW) between 1000 and 1200 g/mol$_{HSO_3}$ were investigated [25]. Table 4.2 gives the specifications of the experimental setup of Andreas et al.

An increase in membrane thickness led to an increase in impedance at low frequencies. The data was fitted to a simple Randles cell model as shown in figure 4.9. The

Table 4.2: Andreaus et al. experimental setup

Experimental Setup	
Type	PEMFC
Active area	28 cm^2
Catalyst loading	0.6 $mgPt/cm^2$
Membrane thickness	Changed
Temperature	80°C
Pressure	1 bar
Current density	$500mA/cm^2$
Frequency	50 mHz - 100 kHz
Reference electrode	No

membrane resistivity increases from 7.42 Ω to 11.01 Ω when the membrane thickness increases from 51 μm to 254 μm. The charge transfer resistance also increases as a function of membrane thickness.

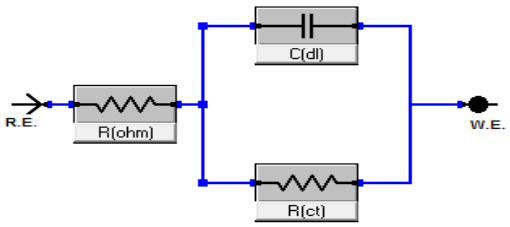

Figure 4.9: Andreaus' cathode equivalent circuit model

The model includes the membrane resistance $R_{(ohm)}$, the double layer capacitance effect $R_{(dl)}$ and the total charge transfer resistance of the anode and cathode $R_{(ct)}$. The oxidation reduction reaction (ORR) (similar to the anode oxygen evolution reaction (OER) in an electrolyser) takes place at the cathode in a fuel cell and is slower than the reaction at the anode. The charge transfer resistance may not only be caused by the ORR at the cathode, but also by the hydrogen oxidation reaction (HOR) at the anode.

Andreaus et al. improved their model to the model shown in figure 4.10. The two

models are almost alike, the only adjustment is the Nernst impedance Z [40].

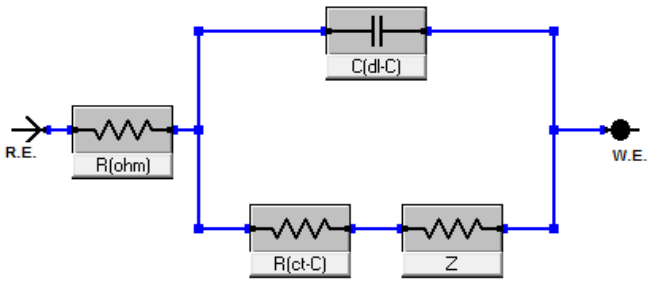

Figure 4.10: Andreaus' equivalent circuit model for a entire fuel cell

The Nernst element Z is in series with the charge transfer resistance $R_{(ct)}$ and represents the mass transport limitation. The mass transport limitation is occurring at low frequencies.

Constant phase element model

Wagner and Gülzow [41, 42] progressively poisoned the fuel cell with carbon monoxide at the anode side. Table 4.3 illustrates the experimental setup used to obtain the model.

Figure 4.11 shows the equivalent circuit model when the anode side is poisoned with carbon monoxide. The poisoning of the anode side causes the charge transfer resistance, of the hydrogen to dominate while the cathode charge transfer resistance is almost constant during the experiment.

In the model R_{el} is the electrolyte resistance, L_k is the pseudo-inductance, R_k is the surface relaxation impedance, R_{ct} is the charge transfer at the anode and the cathode, C_{dl} is the double layer capacitance at the anode and CPE is the constant phase element at the cathode.

Table 4.3: Wagner and Gülzow experimental setup

Experimental Setup	
Type	PEMFC
Active area	23 cm^2
Catalyst loading	20 wt.% Pt/C
Membrane thickness	Nafion 117
Temperature	80°C
Pressure	2 bar
Current density	217 mA/cm^2
Frequency	50 mHz - 10 kHz
Reference electrode	No

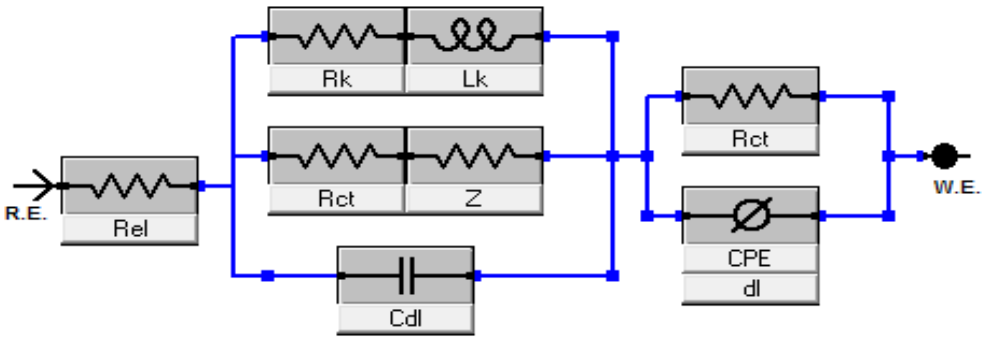

Figure 4.11: Wagner and Gülzow equivalent circuit model

Anode and cathode model

Chiller et al. [43, 44] developed a model based on two different operation modes. First they prevented water to exit a PEMFC while under constant load. The second condition was carbon monoxide poisoning of the platinum on the anode. Table 4.4 illustrates the experimental setup. A model was derived from the data obtained during these tests.

The model is shown in figure 4.12. In this model $R_{(ct-C)}$ and $R_{(ct-A)}$ are the charge transfer resistances associated with the cathode and anode respectively, $Z_{(C)}$ is the

Table 4.4: Chiller et al. experimental setup

Experimental Setup	
Type	PEMFC
Active area	23 cm^2
Catalyst loading	20 wt.% platinum
Membrane thickness	Nafion 117
Temperature	80°C
Pressure	2 bar
Current density 1	87 mA/cm^2
Current density 2	217 mA/cm^2
Frequency 1	10 mHz - 20 kHz
Frequency 2	50 mHz - 10 kHz
Reference electrode	No

finite diffusion impedance, $C_{(dl-C)}$ is the double layer capacitance at the anode, $CPE_{(C)}$ is a constant phase element associated with a porous cathode electrode, $R_{(el)}$ is the resistance of the membrane and $L_{(wir)}$ is the inductance of the conductors.

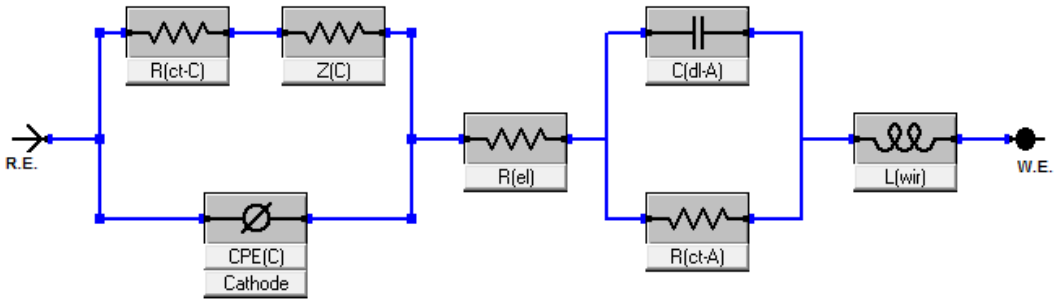

Figure 4.12: Chiller et al. equivalent circuit model for a entire fuel cell

4.3.2 Model development procedure

Randles Cell

The Randles cell is one of the most commonly used equivalent circuit models. The Randles cell is used to form the basis of the equivalent circuit model development. Figure 4.13 shows the Randles equivalent circuit.

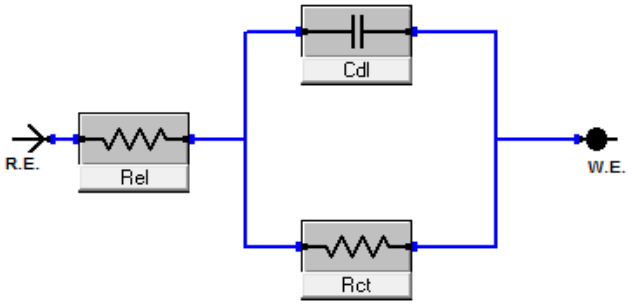

Figure 4.13: Randles cell

The impedance of the Randles cell is:

$$Z(\omega) = R_{el} + \frac{1}{R_{ct}^{-1} + j\omega C_{dl}} \tag{4.1}$$

$$Z(\omega) = R_{el} + \frac{R_{ct}}{1 + j\omega R_{ct} C_{dl}} = R_{el} + \frac{R_{ct}(1 - j\omega R_{ct} C_{dl})}{(1 + j\omega R_{ct} C_{dl})(1 - j\omega R_{ct} C_{dl})} \tag{4.2}$$

$$Z(\omega) = R_{el} + \frac{R_{ct}}{1 + j\omega^2 (R_{ct} C_{dl})^2} - j\frac{\omega R_{ct}(R_{ct} C_{dl})}{1 + j\omega^2 (R_{ct} C_{dl})^2} \tag{4.3}$$

The Randles cell equivalent circuit includes an electrolyte resistance, a double layer capacitor and a charge transfer resistance. The Nyquist plot for a Randles cell is always a semicircle as shown in figure 4.14. The electrolyte resistance value is the intercept with the real axis at high frequencies. This is the intercept near the origin of the plot. The Nyquist plot was generated assuming that R_{el} = 100 mΩ and R_{ct} = 9.8 mΩ.

The real axis value at the other (low frequency) intercept is the sum of the polarization resistance and the solution resistance. The diameter of the semicircle is therefore equal

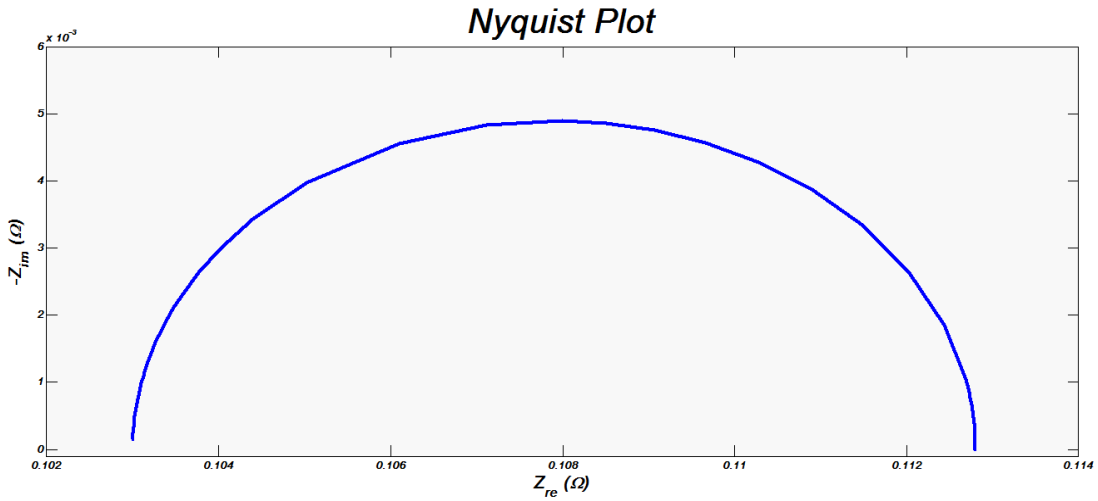

Figure 4.14: The Nyquist plot of the Randles cell

to the charge transfer resistance. The imaginary part of the impedance reaches a maximum point at frequency ω_m and is also known as the characteristic frequency [36]:

$$\omega_m = (R_{ct}C_{dl})^{-1}. \tag{4.4}$$

Model including mass transfer

The Randles cell needs to be modified to accumulate the effect of mass transfer. The Warburg impedance is discussed in section 3.4.3. The mass transfer effect is noticeable at low frequencies. The Warburg impedance is given by

$$Z_\omega = \sigma\omega^{-1/2} - j\sigma\omega^{-1/2}. \tag{4.5}$$

The effect of mass transport is usually seen in a second semicircle or a 45° line after the first semicircle. A second semicircle is associated with finite diffusion and the 45° line is due to the infinite diffusion.

The Warburg impedance was added in series with the charge transport resistance in the Randles cell. Figure 4.15 show the modified equivalent circuit.

The mass transport effect is added by the 45° line shown in the Nyquist plot in figure

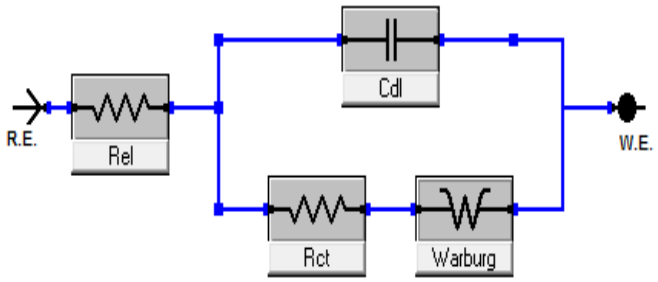

Figure 4.15: Model including mass transfer

4.16. The impedance of the model is given by

$$Z(\omega) = R_{el} + \{j\omega C_{dl} + [R_{ct} + \sigma\omega^{-0.5} - j\sigma\omega^{-0.5}]^{-1}\}^{-1}. \tag{4.6}$$

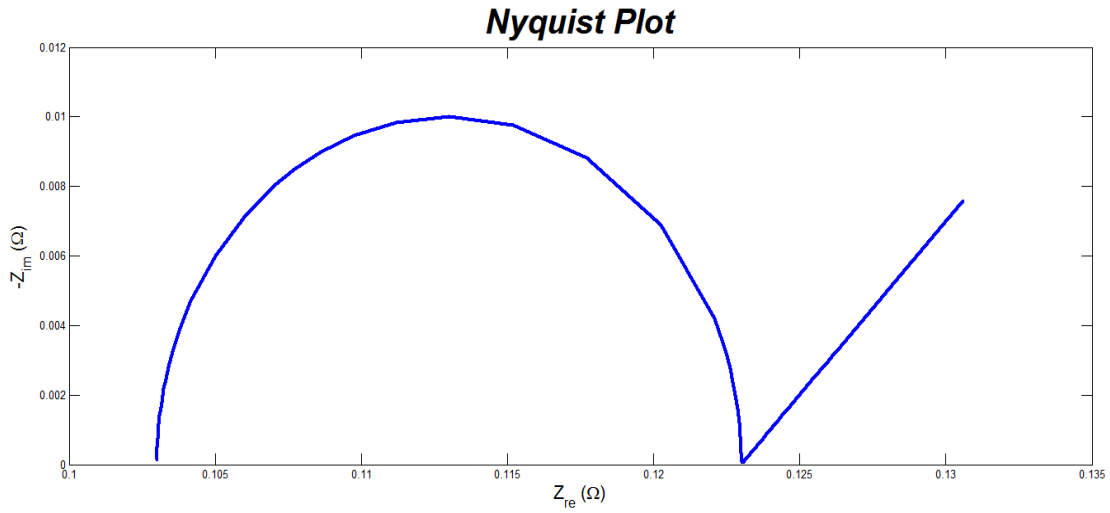

Figure 4.16: Nyquist plot of model which compensate for mass transport effect.

The σ in (4.5) refers to the value of the mass transport effect. The value of the σ was toggled to see how the Nyquist plot was effected. In figure 4.17 the value of σ was changed, the double layer capacitance, electrolyte and charge transfer resistances was left constant. The effect of σ on the Nyquist plot is quite prominent. The 45° line increases as the value of σ increased.

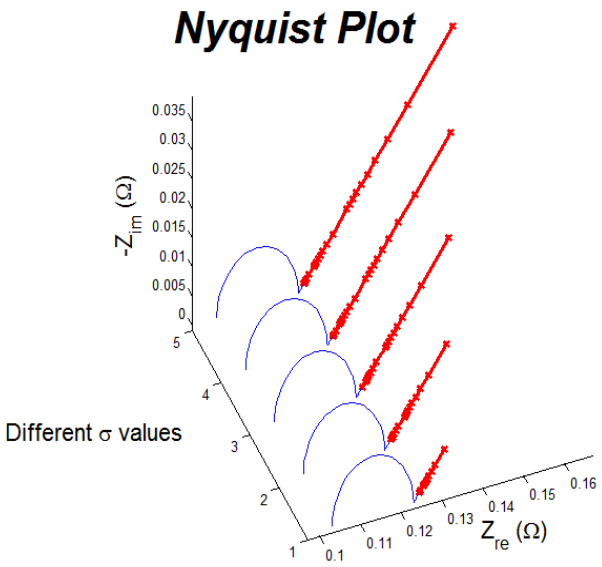

Figure 4.17: The effect of different values for σ in the Warburg impedance

Model with the CPE

Normally the centre of the semicircle of experimental EIS data is not on the real-axis. This effect can be due to several factors including surface roughness, varying thickness or composition and non uniform current distribution. The surface of the electrode is porous and does not act as a pure capacitor. The double layer capacitor does not simulate the effect accurately. A CPE is used to represent the centre of the semicircle below the real-axis.

The CPE is discussed in section 3.4.3. The impedance of the CPE is given by

$$Z_{CPE}(\omega) = \frac{1}{Q(j\omega)^n}. \tag{4.7}$$

The factor of the phase shift is $n \times 90°$. Q is the value of the parameter.

The equivalent circuit model is presented in figure 4.18. The impedance of the model is

$$Z(\omega) = R_{el} + \left\{ Q\omega^n[\cos(\frac{\pi}{2}n) + i\sin(\frac{\pi}{2}n)] + [R_{ct} + \sigma\omega^{-0.5} - i\sigma\omega^{-0.5}]^{-1} \right\}^{-1}. \tag{4.8}$$

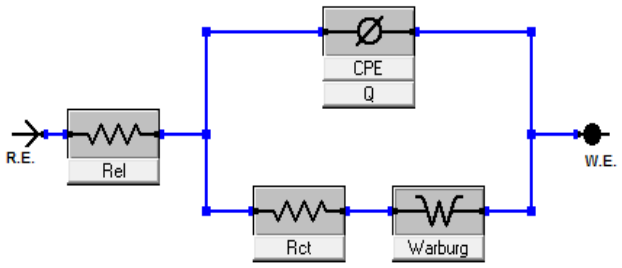

Figure 4.18: Model including a CPE

Figure 4.19 shows the Nyquist plot of the new proposed model. In the previous model the mass transport ($45°$ line) began after the semicircle reaches the real-axis. In the new proposed model the semicircle and the mass transport effect overlap. This is a closer representation of a real system.

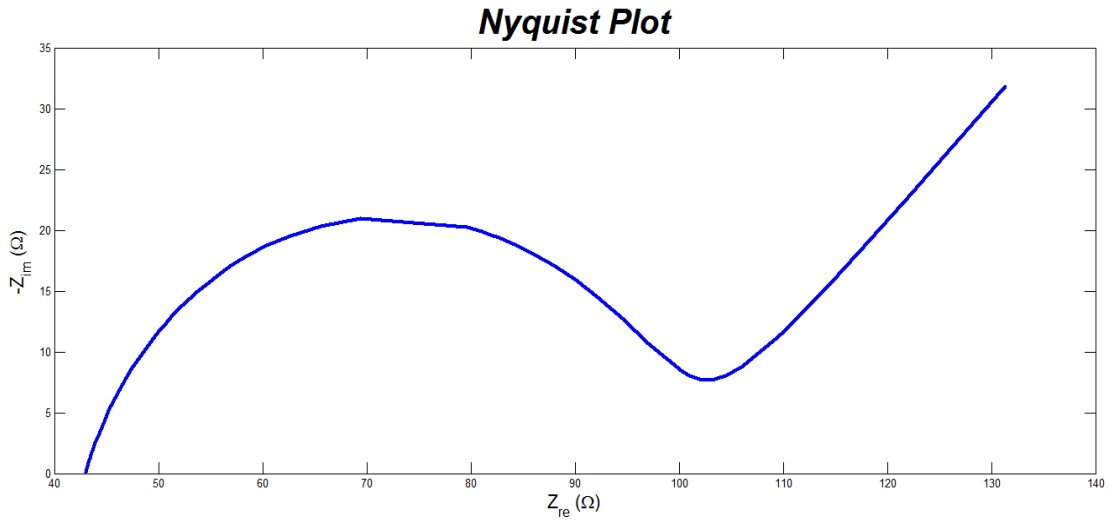

Figure 4.19: Nyquist plot including a CPE

The overlapping section of the semicircle and the mass transport effect (low and high frequency) change with different current densities. If mass transport dominates the system the $45°$ line intercepts the semicircle earlier. The value of Q in the CPE can simulate a similar effect. Figure 4.20 shows the effect on the Nyquist plot if the value of Q is increased. The phase shift in the CPE is due to the factor of n. When $n = 1, 0, -1$ the CPE represent a capacitor, resistor or inductor respectively. The semicircle shifts a $n \times 90°$ factor. The value of n is approximately 0.8. Figure 4.21 shows the Nyquist plot

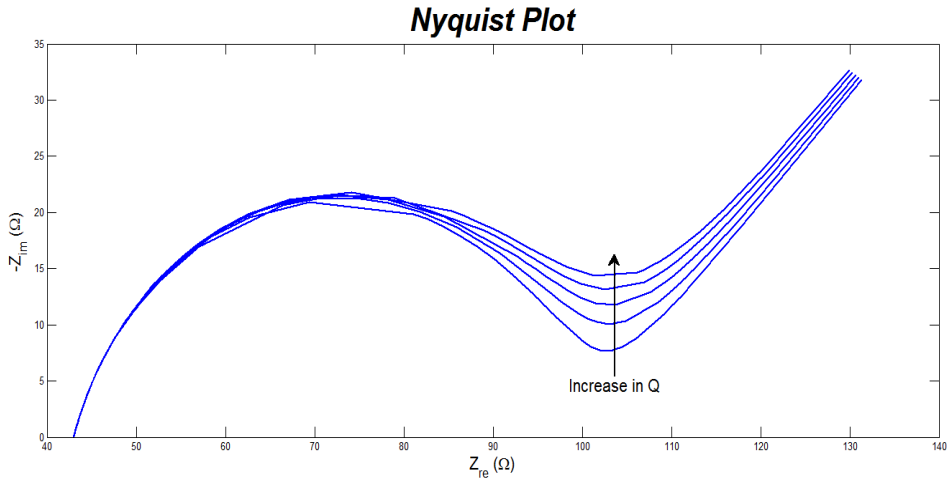

Figure 4.20: Nyquist plot where Q varies

for different values of n. As n is shifted from 0.16 to 0.8 the effect of the phase shift can be seen.

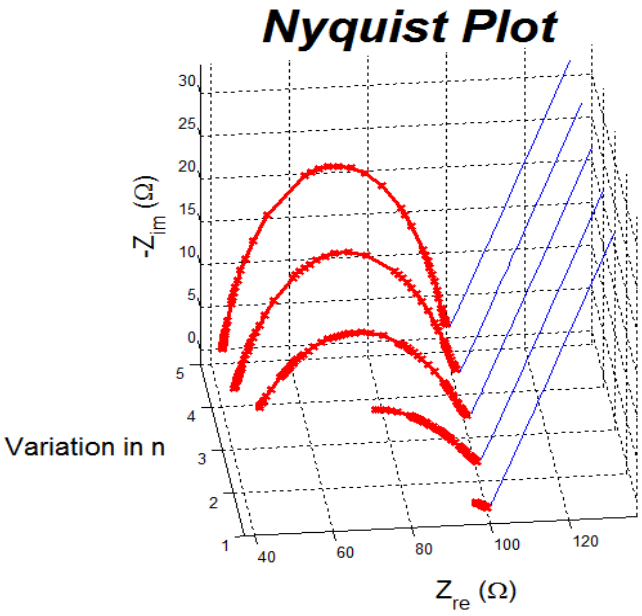

Figure 4.21: Nyquist plot where n varies

Model for the anode and cathode

The previous models proposed were modelled for the electrolyser as a whole. In some cases it is necessary to separate the anode and cathode reactions.

The OER at the anode is the reaction associated with the largest losses while the hydrogen evolution reaction (HER) at the cathode has relatively small losses. Therefore the charge transfer at the anode should be larger than the charge transfer at the cathode due to the slower OER kinetics. In the same matter the CPE of the anode will be larger than the CPE of the cathode. The mass transport effect is added at the anode but is discussed in the next section. The ohmic losses will be due to the membrane resistance. A small inductance is added to the circuit to represent the small inductance associated with the conductors. Figure 4.22 shows the model where the anode is separated from the cathode. The impedance of the model is given by

$$Z(\omega) = \left\{ Q_{anode}\omega^{n_{anode}}[\cos(\frac{\pi}{2}n_{anode}) + j\sin(\frac{\pi}{2}n_{anode})] + [R_{ctanode} + \sigma\omega^{-0.5} - j\sigma\omega^{-0.5}]^{-1} \right\}^{-1}$$

$$+j\omega L + R_{el} + \left\{ Q_{cathode}\omega^{n_{cathode}}[\cos(\frac{\pi}{2}n_{cathode}) + j\sin(\frac{\pi}{2}n_{cathode})] + [R_{ctcathode}]^{-1} \right\}^{-1}. \quad (4.9)$$

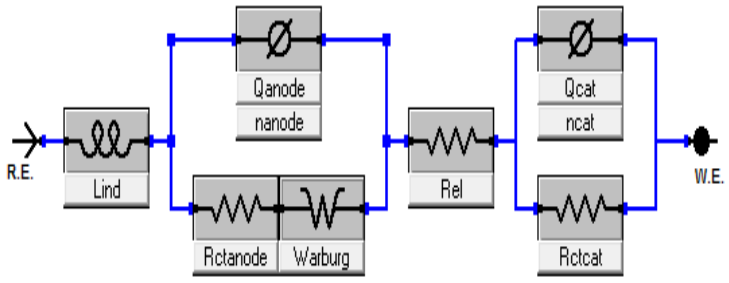

Figure 4.22: Model for the anode and cathode

The Nyquist plot is shown in figure 4.23. The Nyquist plot has two semicircles, the first small semicircle is due to the HER at the cathode. The larger semicircle represents the OER at the anode. This effect is only seen if the kinetics of the HER at the cathode is slow. The effect is not common because the OER has slower kinetics than the HER.

Final equivalent circuit model

The ohmic, activation and mass transfer losses take place in a PEM electrolyser. The effect of each loss is present in the equivalent circuit model. The experimental

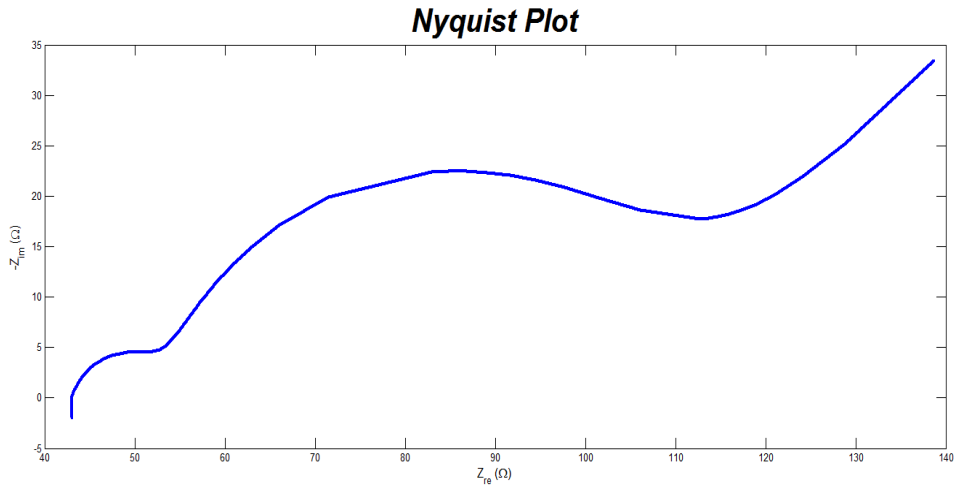

Figure 4.23: Model that separate the effect of the anode and cathode

results show an inductive effect at high frequencies. Figure 4.24 shows the proposed equivalent circuit model.

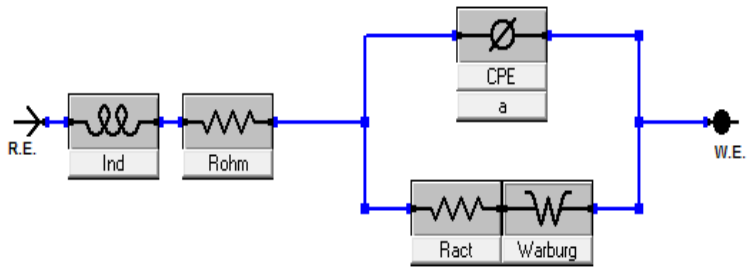

Figure 4.24: The final equivalent circuit model

The ohmic resistance, R_{ohm} describes the ohmic losses of the whole cell. The resistance of the conductors, membrane and the contact resistance is measured with the EIS technique. The inductance of the conductors is presented by I_{nd}.

The middle section of the equivalent circuit model in figure 4.24 describes the activation losses. The activation losses, R_{act} are due to the kinetics of the two reactions at the anode and cathode. The OER at the anode is slower than the HER at the cathode and therefore the losses at the cathode are considered to be negligible. CPE and a are parameters of the CPE and are discussed in section 3.4.3.

The mass transfer effect is associated with W_{arburg}. The mass transport was originally added to the anode side but the production and diffusion of hydrogen at the cathode

side dominates the mass transfer effect. An infinite Warburg parameter is present in the model.

The equivalent circuit model in figure 4.24 will be used as the proposed equivalent circuit model. The verification and validation of the equivalent circuit model is done using this equivalent circuit model.

4.4 Data fitting method

The parameters of the equivalent circuit model (section 4.3) need to characterise the PEM electrolyser. The equivalent circuit model is fitted to the experimental EIS data (section 4.2) to generate parameter values for the equivalent circuit model.

A graphical method was used to analyse the data before computer technology was developed. This method is applied in many diagnostic applications where only the values of a few frequencies are monitored. With the development of technology a more effective approach is developed. The experimental data is fitted to the equivalent circuit model.

The use of computer based EIS analysis software enhances the use of equivalent circuit models [45]. Most of the software use a non-linear least squares (NLLS) fitting method. The method was developed by Marquardt and Levenberg and the Levenberg-Marquardt algorithm has become a commonly used algorithm.

The NLLS Levenberg-Marquardt algorithm uses the chi-squared parameter

$$\chi^2 = \sum_{j=1}^{n} \left(\frac{(y_j - f(x_j))}{\sigma_j} \right)^2, \tag{4.10}$$

where σ_j is the standard deviation, y_j the data and $f(x_j)$ the known function [46]. The function $f(x_j)$ represents the equivalent circuit model. The value of the chi-squared function, χ^2 indicates the difference between the value of the data and the value of the function. The objective is to minimise the chi-squared function, χ^2. The χ^2, function represents the accuracy of the fit. The equivalent circuit model is used in the Gamry

software, Echem Analyst. A Levenberg-Marquardt fitting algorithm is used to fit the data to experimental data in the Gamry environment.

4.5 Conclusion

This chapter discussed two separate processes being developed in parallel. The experimental procedure is used to acquire experimental results while an equivalent circuit model is developed to fit the experimental results.

The experimental setup includes critical aspects necessary to perform EIS on PEM electrolysers. The EIS experimental results are interpreted by using Nyquist plots showing the impedance at different frequencies.

The equivalent circuit model was developed to represent the PEM electrolyser. The equivalent circuit model in figure 4.24 will be used to characterise PEM electrolysers. This specific equivalent circuit model was developed to represent the three main losses in the most elementary way while adding the Warburg and CPE elements. The equivalent circuit model is verified by charactersing a single MEA. The validation of the model was done by charactersing multiple MEAs.

The equivalent circuit model has been developed in this chapter. The verification and validation of the equivalent circuit model is the focus of the next two chapters.

CHAPTER 5

EQUIVALENT CIRCUIT MODEL VERIFICATION

5.1 Introduction

This chapter verifies the EIS results of the characterisation process of a PEM electrolyser. The ohmic, activation and mass transfer losses are the most prominent losses in a PEM electrolyser. A parametric study for each of the losses is done by changing a component or condition responsible for the loss. The membrane thickness was varied in the membrane electrode assembly (MEA) to identify the ohmic loss. The temperature was changed to capture the activation losses. Two different diffusion media were used to investigate the mass transfer effect. EIS was applied to the PEM electrolyser and the ohmic, activation and mass transfer losses were identified. The EIS results were confirmed with other electrochemical methods like polarisation curves and Tafel plots.

5.2 Ohmic losses

The ohmic resistance in a PEM electrolyser refers to the resistance which is caused due to the current flow through the cell. The ohmic resistance includes the contact

resistance, grain-boundary resistance, membrane resistance as well as the resistance of the catalyst layers. Although all these resistances are present, the resistance of the proton exchange membrane contributes the most of the total ohmic resistance.

The effect of ohmic resistance was investigated with three MEAs with different membrane thickness. MEAs with N115 (127 microns), N117 (183 microns) and N1110 (254 microns) membrane thickness was used. The electro-catalyst loading on the three MEAs are the same. The operating conditions and cell hardware (like the GDLs) was kept the same for all three MEAs.

5.2.1 EIS results for the ohmic losses

Figure 5.1 depicts the Nyquist plot of the three MEAs. EIS was applied while the PEM electrolyser was operated at 1 A/cm^2 and at 60 °C. At high frequencies the capacitances in the system acts as a short circuit and only the ohmic resistance is measured. The ohmic resistance is determined from the high frequency intercept on the real axis in the Nyquist plot.

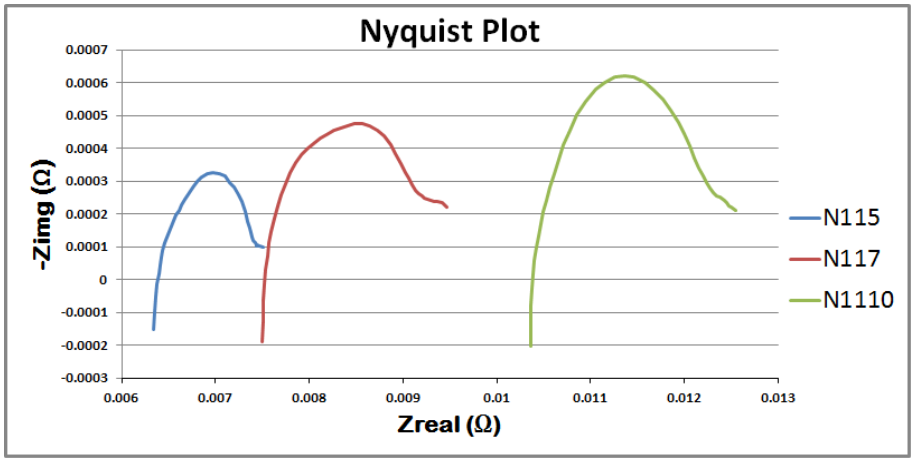

Figure 5.1: Nyquist plots of different membrane thickness at 60 °C

The N115, N117 and N1110 ohmic resistance is 6.39 mΩ , 7.54 mΩ and 10.39 mΩ respectively. The membrane thickness of the MEA has an effect on the ohmic resistance. The thinner membrane has the smallest ohmic resistance and the thicker membrane the largest. This phenomenon was also seen in the literature [24, 25].

5.2.2 Verification method for the ohmic losses

To verify the EIS results for the ohmic losses the polarisation curve was used. The current-voltage relation is shown in figure 5.2. The thinner membrane (N115) shows the best performance while the thicker (N1110) has the highest overpotential. The slope difference is due to the increase in ohmic resistance. The DC resistance is calculated using ohm's law from the polarisation curve at 1 A/cm^2.

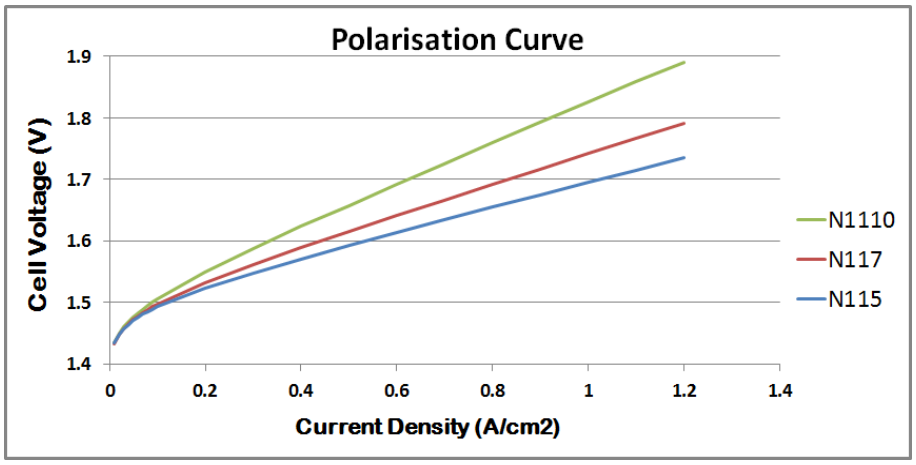

Figure 5.2: Polarisation curve of different membrane thickness at 60°C

The difficult part is to compare the EIS ohmic resistance with the resistance calculated with the polarisation curve. This is due to the fact that EIS measures the ohmic resistance in the frequency domain while the polarisation curve measurements are in the time domain. The DC resistance calculated with the polarisation curve can be achieved with EIS when very low frequencies are applied in the method [47]. The equipment available is unable to operate at these low frequencies.

Table 5.1 shows the DC (polarisation curves) and AC (EIS) resistances of the whole cell. The trend of the two methods is compared by calculating the total increase of resistance from the N115 membrane to the N1110 membrane. The increase in resistance from N115 to N117 and N117 to N1110 and the percentage of the total increase of the resistance is calculated. A trend of 36 % and 64 % for the polarisation curve and 29 % and 71 % for EIS resistance is calculated.

Table 5.1: Ohmic resistance

Membrane	Measuring method					
	Polarisartion curve			EIS		
	R_{dc} (Ω)	(Ω)	(%)	R_{ac} (Ω)	(Ω)	(%)
N115	1.697			0.00639		
Increase in resistance		0.0469	36%		0.00114	29%
N117	1.744			0.00754		
Increase in resistance		0.0834	64%		0.00285	71%
N1110	1.827			0.01039		

5.2.3 Identifying membrane and catalyst resistances with EIS

With the increase of membrane thickness the membrane resistance can be calculated as the intercept with the real axis in the Nyquist plot. Figure 5.3 shows the resistance versus membrane thickness.

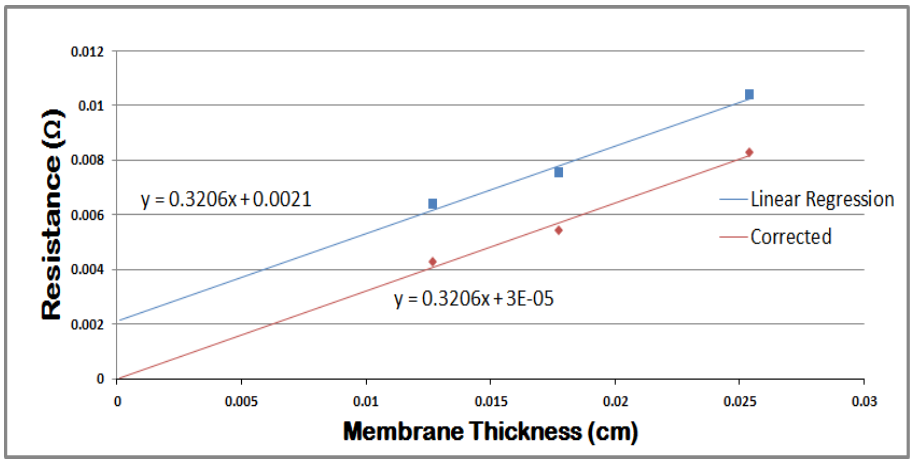

Figure 5.3: Resistance related to membrane thickness

A trend line can be constructed to indicate the resistance related to the membrane thickness. At zero thickness the resistance should also be zero if the resistance was only dependant on the membrane resistance. The resistance of 2 mΩ is the resistance

of the catalyst layers on both sides of the membrane.

The equivalent circuit model can be reconstructed and the ohmic resistance can be categorised into the membrane and catalyst resistance. Figure 5.4 shows the equivalent circuit model.

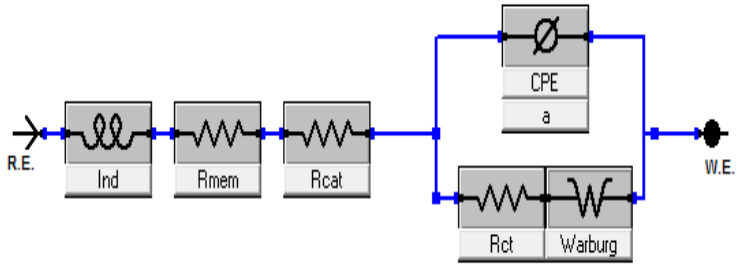

Figure 5.4: Equivalent circuit model

In table 5.2 the three MEAs are evaluated. The resistance of the membranes were calculated by identifying the catalyst resistance and subtracting it from the ohmic resistance. The conductivity of the membrane N115, N117 and N1110 are 0.119 S/cm, 0.131 S/cm and 0.123 S/cm respectively. The conductivity of the membrane recorded in the literature is between 0.1 S/cm and 0.35 S/cm [48]. The conductivity results of the membrane are close the the lower limit and still in the range found in the literature.

Table 5.2: Identifying the membrane and catalyst resistance

	Nafion 115	Nafion 117	Nafion 1110
Membrane thickness (cm)	0.0127	0.01778	0.0254
EIS resistance (mΩ)	6.38	7.52	10.39
Catalyst resistance (mΩ)	2.1	2.1	2.1
Membrane resistance (mΩ)	4.28	5.42	8.29
Membrane conductivity (S/cm)	0.119	0.131	0.123

5.3 Activation losses

The charge transfer resistance is the resistance of the barrier through which the electrons pass through from the electrode surface to the adsorbed species, or from the species to the electrode. Put differently, this is the loss which electrons need to overcome to cross the interface.

The effect of the activation losses was investigated by changing the operating temperature. Only the temperature was changed and an MEA with a N117 membrane was used. An increase in temperature will increase the conductivity of the membrane leading to a smaller ohmic loss. The effect of temperature should not influence the activation energy needed. Thus a change in ohmic resistance is expected while the activation resistance should remain the same.

The single cell was tested at 60 °C, 70 °C and 80 °C and at atmospheric pressure. The best performance at high current densities was obtained at 80 °C. At higher temperatures above 80 °C membrane hydration effects cause a rise in the potential and the ohmic resistance increases with the conventional PEM [49].

5.3.1 EIS results for the activation losses

The Nyquist plots at 60-80 °C in figure 5.5 show semicircles which involve several processes including the activation resistance [50]. The ohmic resistance, already determined in section 5.2, is visible at the high frequency intercept with the real axis. The activation resistance is obtained by the difference between the low frequency and high frequency intercept with the real axis [50]. The activation resistance calculated decreased from 1.93 mΩ to 1.78 mΩ.

5.3.2 Verification method for the activation losses

The verification of the EIS results is done by means of Tafel plots. The electrode reaction kinetics can be investigated using the Tafel plot. The Tafel slope gives the amount of

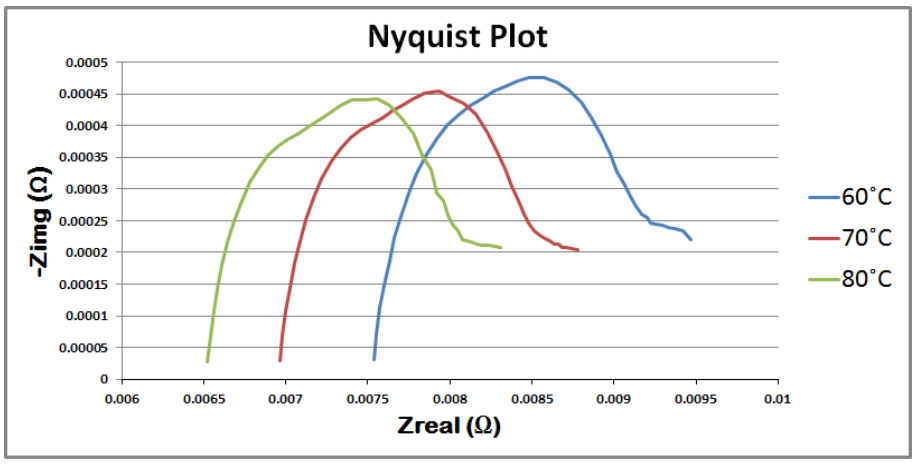

Figure 5.5: Nyquist plot of the N117 at 60 °C, 70 °C and 80 °C

activation resistance needed to achieve the current density. The smaller the Tafel slope the better the performance of the cell.

The data acquired to perform Tafel plots are obtained at low current densities (low current density range of the polarisation curve). At low current densities the mass transfer effects are minimised. The theoretical Tafel slope,

$$b$$

in V/dec, is defined as

$$b = 2.303\frac{R \cdot T}{a_c \cdot n \cdot F}, \tag{5.1}$$

where a_c is the transfer coefficient, n is the number of electrons to complete the reaction, F is Faraday's constant (96486 C/equiv.), R is the ideal gas constant (8.314 J/mole °K) and T is the absolute temperature (°K). In a PEM fuel cell the theoretically calculated cathodic Tafel slope is 70 mV/dec at 80 °C [36].

Figure 5.6 shows the Tafel plots in the low current density regions of 60 °C, 70 °C and 80 °C. The observed Tafel slopes were close to 80 mV/dec. A Tafel slope of 80 mV/dec for water electrolysis is typically observed and includes both the anode (50 mV/dec) and cathode (30 mV/dec) side [51].

The tafel slope in figure 5.6 increases from 81 mV/dec to 85 mV/dec. This is likely related to ohmic resistance since there was no compensation for IR voltage losses. IR corrected Tafel plots are used in the literature [50, 51]. The IR corrected polarisation

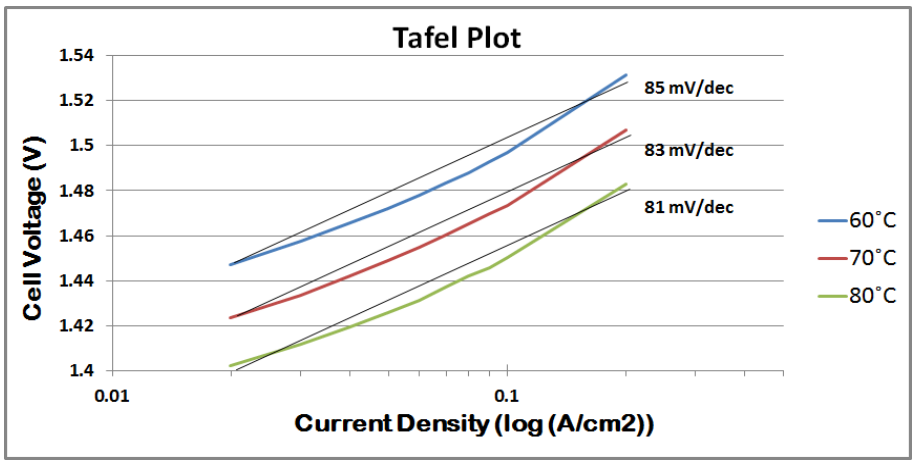

Figure 5.6: Tafel plot of the N117 at 60 °,70 ° and 80°C

curve only includes the effective potential, E_{eff}. The potential caused by the electrolyte resistance is subtracted as shown in 5.2.

$$E_{eff} = E_{applied} - iR, \tag{5.2}$$

where $E_{applied}$ is the applied potential, i is the faradaic current, and R is the electrolyte resistance. Ohmic losses (IR) corrected tafel plots were not used in this study.

5.4 Mass transfer losses

The electrochemical reactions occurring at the electrode surface involve the water that needs to reach the electro-catalyst, where it is split into hydrogen and oxygen. The electro-active species (water) needs to reach the electrode surface. Then these electro-active species need to be absorbed at the electrode/electrolyte interface. Mass transfer occurs when the reactant that reaches the electrode surface is consumed immediately resulting in insufficient reactant on the electrode surface. This means the electrochemical process uses more reactants than can be supplied. Mass transfer also occurs when the products produced are not diffused away fast enough.

In this section the effect of mass transfer was investigated by operating the single cell PEM electrolyser with two different anode GDLs. The operating conditions of 60 °C

and atmospheric pressure was the same in both experiments. The same MEA with N115 membrane was used in both experiments. Two different gas diffusion media was used, carbon paper and platinised titanium.

5.4.1 EIS results for the mass transfer losses

Figure 5.7 shows the Nyquist plot of the two GDLs. The effect of mass transport is usually seen in a second semicircle or a 45° line after the first semicircle. A second semicircle is associated with finite diffusion and the 45° line is due to infinite diffusion [52].

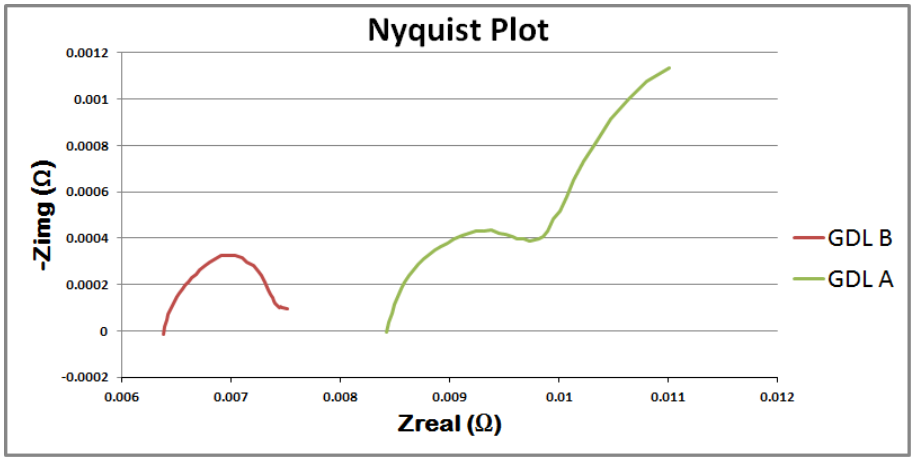

Figure 5.7: Nyquist plot with different GDLs

There does not form a second semi-circle with GDL B. The line at the end of GDL A indicates a significant amount of mass transfer. The ohmic resistance of GDL A is also higher, this will be discussed in the next chapter.

5.4.2 Verification method for the mass transfer losses

The verification is done with polarisation curves. Figure 5.8 shows the polarisation curves of the PEM electrolyser performances with two different GDLs. At higher current densities the cell voltage of GDL A starts to increase exponentially. The GDL B just seems to increase linearly, meaning that only ohmic resistance is present.

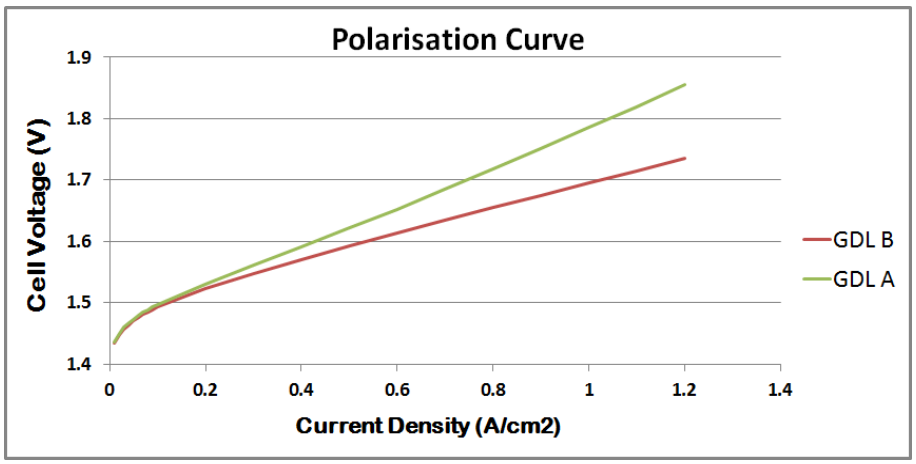

Figure 5.8: Polarisation curve with different GDLs

5.5 Equivalent circuit model

The impedance data collected when EIS is performed can be fitted to an equivalent circuit model. The purpose of the components included in the equivalent circuit model is to represent the processes in a single cell PEM electrolyser. Figure 5.9 shows the equivalent circuit model.

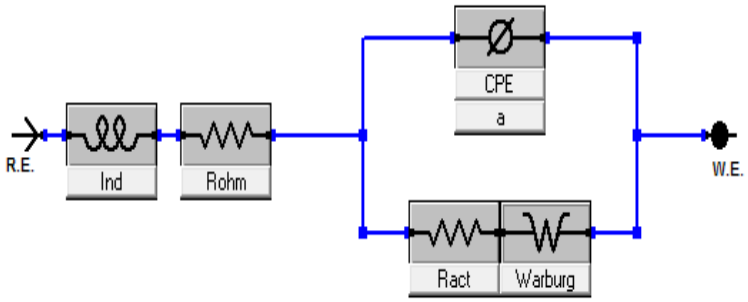

Figure 5.9: Equivalent circuit model

The inductance of the conductors has a effect on the impedance measurement and is simulated using the I_{nd} parameter in figure 5.9. The ohmic resistance is represented by R_{ohm}. The activation resistance R_{act} is the resistance associated with the electro-catalyst activity. The constant phase element (CPE) can be associated with surface roughness, varying thickness or non-uniform current distribution [36]. The Warburg impedance is related to the mass transfer effect in the single cell PEM electrolyser.

Table 5.3: Equivalent circuit model parameters

	R_{ohm}	R_{act}	Ind	CPE	$Warburg$	
	(mΩ)	(mΩ)	(nH)	(mSs^a)	(k$Ss^{0.5}$)	Goodness of fit
N115	6.367	1.123	7.496	37.22	15	8.899e^{-6}
N117	7.376	1.99	20.15	30.57	4.5	3.605e^{-6}
N1110	10.32	2.077	16.44	18.24	4.01	1.273e^{-6}

In Table 5.3 the values of the fitted equivalent circuit model are given for the membranes operated at 60 °C and 1 A/cm^2. The Nyquist plots are illustrated in figure 5.10.

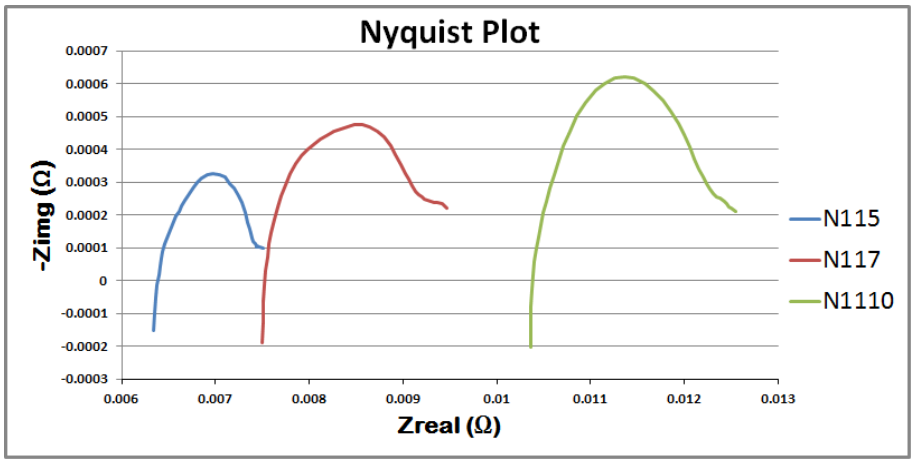

Figure 5.10: Nyquist plots of different membrane thickness at 60 °C

The increase in membrane thickness is perfectly modelled by showing an increase in the ohmic resistance within the model parameters. A small increase in the activation resistance is modelled. This should be the same for all three membranes. A possible explanation can be the influence of the ohmic resistance. The CPE values represent the shape of the semicircle. The high Warburg values illustrates that there is no mass transfer occurring.

5.6 Conclusion

A parametric study was done in the verification process of the equivalent circuit model. The ohmic, activation and mass transfer losses were identified with the equivalent circuit model and verified with other electrochemical techniques.

The ohmic resistance was identified by using different membrane thicknesses. The equivalent circuit showed an increase in ohmic resistance as the membrane thickness increased. The ohmic resistance was further investigated by identifying the catalyst resistance. The equivalent circuit model was reconstructed and the membrane resistance and catalyst resistance is now present. This adds new value to EIS as an electrochemical technique, although three or more MEAs are needed to get these results.

The activation losses were identified by changing the operating temperature. The activation resistance shows a slight decrease when calculated with the equivalent circuit model. The Tafel plots of the MEAs at different temperatures also shows a slight decrease.

The effect of mass transfer was seen when two different GDLs were used. The equivalent circuit model was applied and the performance evaluated with the goodness of the fit which was between $1.273e^{-6}$ and $8.899e^{-6}$. The results were verified with the polarisation curves and Tafel plots.

CHAPTER 6

EQUIVALENT CIRCUIT MODEL VALIDATION

6.1 Introduction

This chapter will focus on the validation of the equivalent circuit model. The verification process in chapter 5 showed that the equivalent circuit model is capable of characterising a single PEM electrolyser. Part of the validation process is to indicate that the equivalent circuit model can be used to characterise multiple MEAs. Three different MEAs from three different suppliers are characterised by fitting the equivalent circuit model to the experimental EIS data.

The second part of the chapter is dedicated to identifying the optimum operating area. The optimum operating area is derived by identifying the losses with the equivalent circuit model by fitting it to experimental EIS data at different current densities.

The last part of the chapter characterises a component of the PEM electrolyser. Usually the focus is on developing MEAs and the PEM cell hardware is often forgotten. The equivalent circuit model is capable of characterising the effects of hardware components of the PEM electrolyser. Two GDLs are tested and fitted to the equivalent circuit model.

6.2 Characterisation of three different MEAs

The equivalent circuit model is used to characterise one MEA in chapter 5. The ability to characterise different MEAs with different characteristics is part of the validation process.

Three MEAs from three different suppliers was characterised. The same single cell hardware was used to test the MEAs. The MEAs have the same membrane thickness but are different in terms of the electro-catalyst itself and the loading of the electro-catalyst on the membrane. Figure 6.1 shows the polarisation curve of the three suppliers.

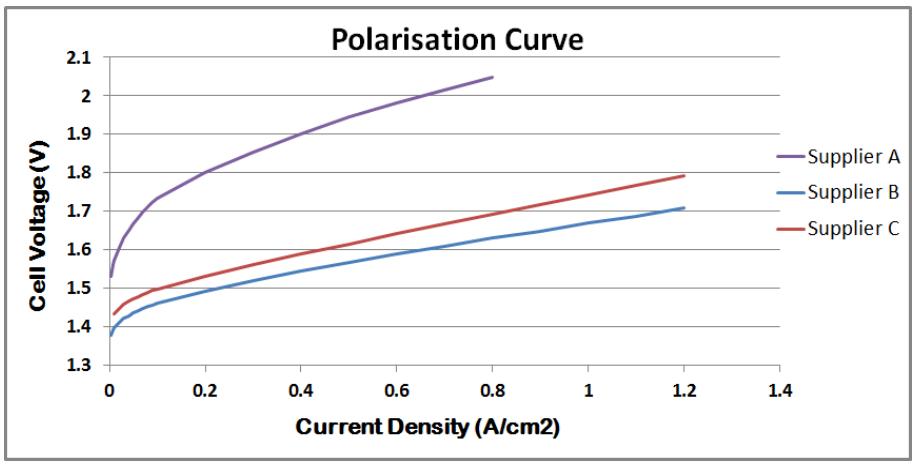

Figure 6.1: Polarisation curves of the three MEA suppliers

Supplier A shows a high overpotential and the experiment was aborted at 0.8 A/cm^2 because of corrosion issues at potentials above 2V. Supplier B and C showed better performances with relative low overpotentials at 60 °C. The Nyquist plots of the three different MEAs are shown in figure 6.2.

The Nyquist plot can identify the different losses in the three MEAs. In the next section the equivalent circuit model will be fitted to the experimental EIS data.

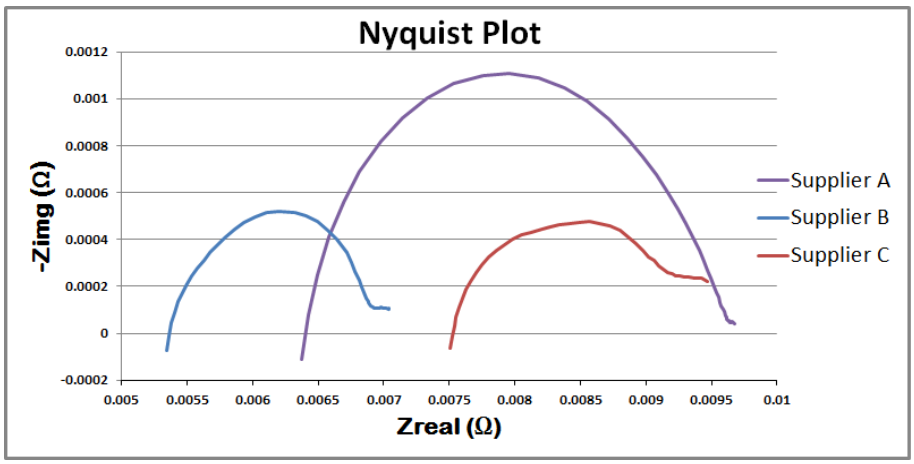

Figure 6.2: Nyquist plot of the three MEA suppliers

6.2.1 Equivalent circuit model fitting

The equivalent circuit model developed in chapter 4 is used to characterise the three different MEAs. Figure 6.3 shows the equivalent circuit model.

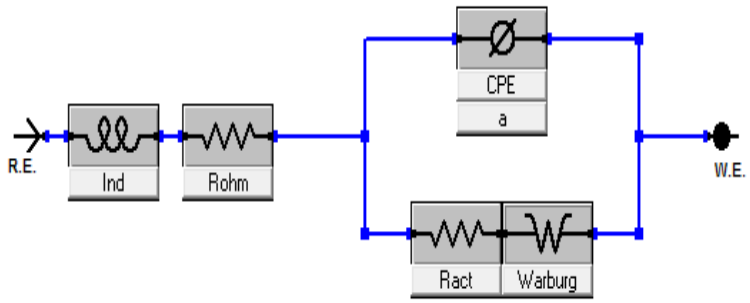

Figure 6.3: Equivalent circuit model

The I_{nd} parameter represents the inductance of the system. The PEM electrolyser has very little inductance and most of the inductance is due to the conductors of the potensiostat. The ohmic resistance of the whole system is presented by R_{ohm}. The activation resistance R_{act} is related to the activation energy of the electro-catalyst. The two CPE parameters, CPE and a compensate for the unique form of the semi-circle. The Warburg parameter indicates the mass transfer factor.

The electro-catalyst used in the MEA of supplier A is called Pt black (platinum black). The Pt black powder is either sprayed or hot pressed onto the membrane to form the

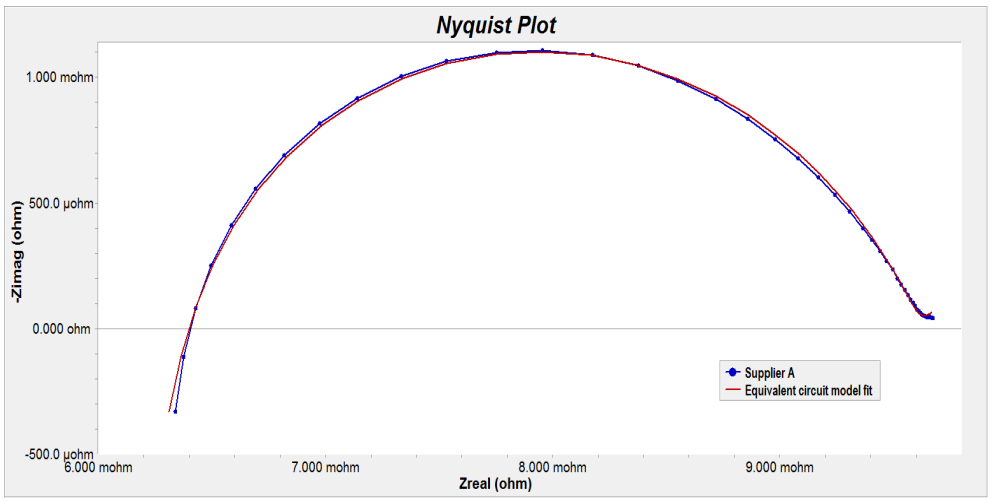

Figure 6.4: Nyquist plot of supplier A

MEA. The loading of the Pt black electro-catalyst on the MEA is 4.5 mgPt/cm^2 on the anode side and 4 mgPt/cm^2 on the cathode side. Figure 6.4 shows the Nyquist plot of the fitted equivalent circuit model of supplier A. The parameter values are presented in table 6.1.

Iridium-ruthenium oxide (IrRuOx) is the anode electro-catalyst of supplier B. IrRuOx is known for fast kinetics and the electro-catalyst loading is 3 mgIrRuOx/cm^2 on the anode side and 3 mgPtB/cm^2 on the cathode side. The equivalent circuit model is fitted to the experimental EIS data. The Nyquist plot is shown in figure 6.5. The parameter values are presented in table 6.1.

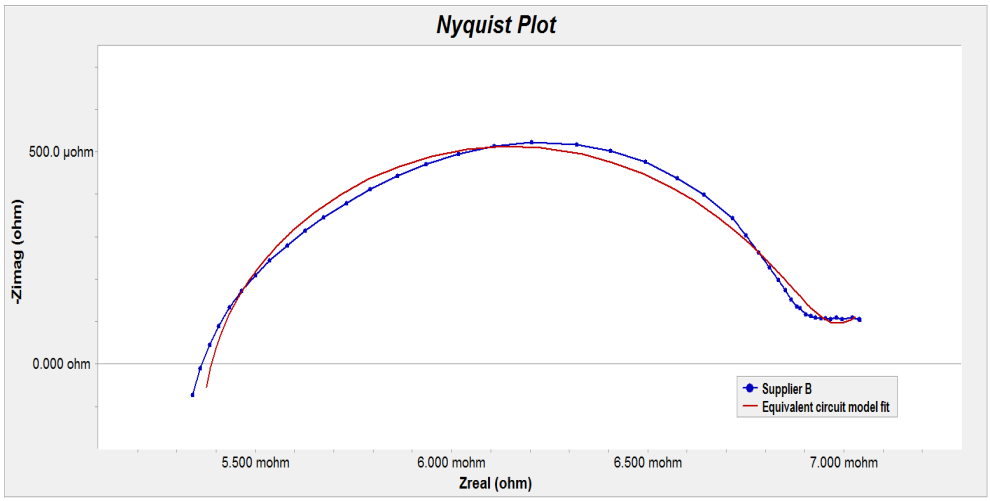

Figure 6.5: Nyquist plot of supplier B

The electro-catalyst used in the MEA of supplier C is Iridium oxide (IrOx). A loading of 1 mgIrOx/cm^2 is used on the anode and on the cathode side 0.3 mgPt/cm^2 is used because the HER is faster than the OER at the anode. Figure 6.6 shows the Nyquist plot of the equivalent circuit model fitted to the experimental EIS data. The parameter values are presented in table 6.1.

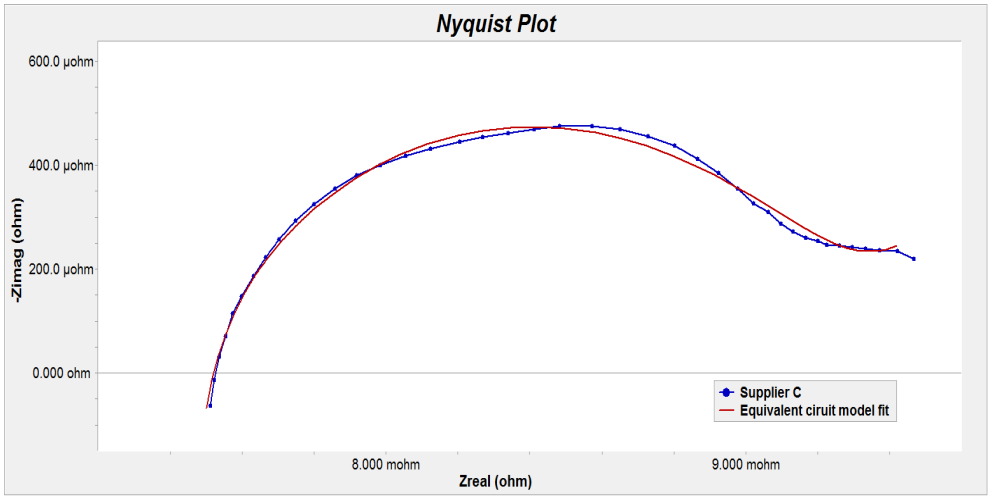

Figure 6.6: Nyquist plot of supplier C

The parameters of the fitted equivalent circuit model is present in table 6.1. The fitted model and the experimental results is shown in figures 6.4 - 6.6.

The ohmic resistance measured with EIS is the resistance of the whole system and not only the membrane resistance. The membrane resistance and the electro-catalyst can be separated if different membrane thicknesses were tested as was shown in section 5.2.3. The small difference in ohmic resistance of the MEAs is due to the different electro-catalyst layers because the same N117 membranes was present in all the MEAs. The behaviour of supplier B and C in figure 6.1 are the same and the slightly higher overpotential of supplier C is the slightly higher ohmic resistance.

The activation resistance, R_{act} is the resistance an ion experiences to cross the interfaces. The kinetics of the electro-catalyst determine the activation resistance of the MEA. The activation resistance of the MEA of supplier A is 3.55 mΩ. This value is high in terms of the other two MEAs. The Tafel plot in figure 6.7 indicates a Tafel slope of 160 mV/dec for the MEA. A typical water electrolysis slope should be around 80 mV/dec which

Table 6.1: Equivalent circuit model parameters for the three MEAs

	R_{ohm} (mΩ)	R_{act} (mΩ)	CPE (Ss^a)	a ( )	$Warburg$ (k$Ss^{0.5}$)	I_{nd} (nH)	Goodness of fit
Supplier A	6.06	3.55	0.702	0.732	12.3	14.7	2.18e-6
Supplier B	5.32	1.63	8.47	0.716	7.87	7.87	14.63e-6
Supplier C	7.38	1.98	30.3	0.565	4.43	19.4	3.37e-6

explains the high overpotential of supplier A in figure 6.1. The activation resistance of 1.63 mΩ and 1.98 Ω of supplier B and C correlate to the Tafel slope of 72 mV/dec and 84 mV/dec shown in figure 6.7.

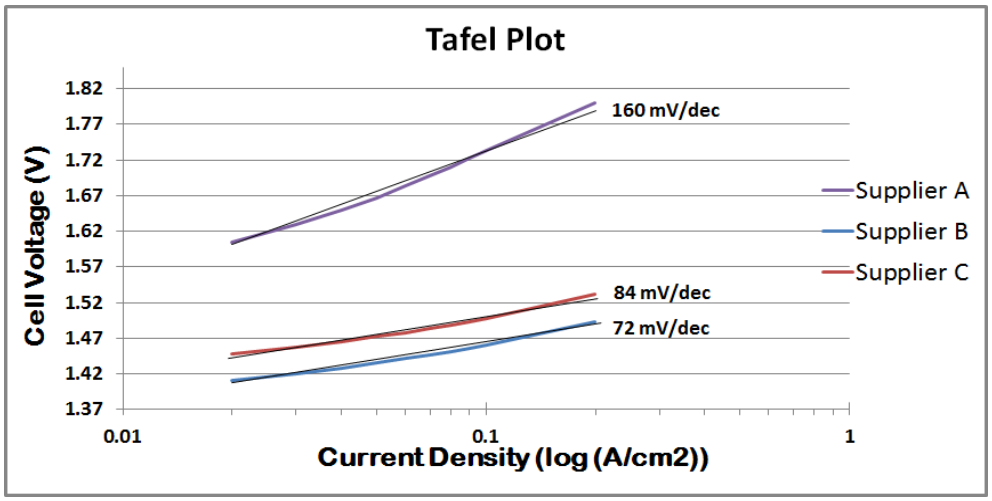

Figure 6.7: Nyquist plot of the three MEA suppliers

The constant phase element parameters, CPE and a relates to the shape of the semicircle. The CPE parameter states the region where the semicircle overflow to the low frequency region (mass transport). The a parameter indicates the semicircle as discussed in section 4.3.2. This a parameter refers to fractional calculus. These two parameters are not related to any of the main losses but can be seen as an tool to fit the experimental data.

The mass transfer effect is usually a second semicircle of 45° line following the first

semicircle. The experiment EIS data have no mass transfer limitations. A large Warburg parameter value indicates little or no mass transfer effect.

6.3 Optimum operating area

An important aspect of any system is to operate at the optimum efficiency. In a PEM electrolyser many operating conditions like temperature, pressure and the flow of water have an influence on the performance. Many studies have been done to find the optimum operating conditions in terms of the temperature, pressure and flow of water. This section identifies the optimum operating point regarding to the losses at different current densities.

EIS data was captured at different current densities to investigate the ohmic, activation and mass transfer resistances. Figure 6.8 shows the Nyquist plot at different current densities.

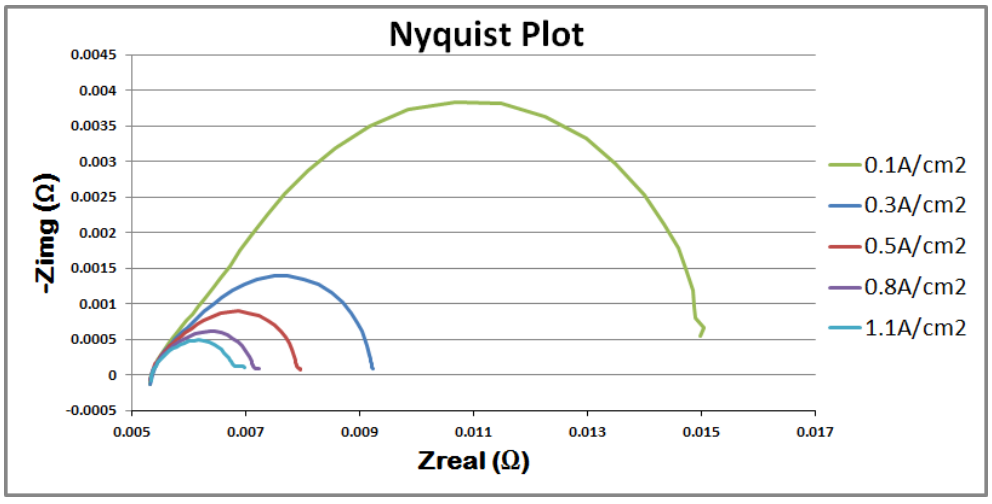

Figure 6.8: Nyquist plot at different current densities

The equivalent circuit model is fitted to experimental EIS data at different current densities. The equivalent circuit model parameters are shown in table 6.2.

The ohmic resistance measured with EIS over the current density range stays steady around 5.49 mΩ. This response is ascribable to the fact that the ohmic resistance

Table 6.2: Equivalent circuit model parameters at different current densities

	R_{ohm} (mΩ)	R_{act} (mΩ)	CPE (Ss^a)	a ( )	$Warburg$ (k$Ss^{0.5}$)	Ind (nH)	Goodness of fit
0.1 A/cm^2	5.50	10.29	9.685	0.762	1408	10.4	1.883e-3
0.3 A/cm^2	5.49	3.86	8.002	0.774	44.6	10.3	1.508e-3
0.5 A/cm^2	5.48	2.48	6.711	0.798	42.7	10.2	1.617e-3
0.8 A/cm^2	5.48	1.67	5.597	0.829	8.3	10.2	1.679e-3
1.1 A/cm^2	5.49	1.31	4.958	0.851	4.06	10.2	1.673e-3

measured with EIS include the membrane and electro-catalyst resistance, which stays the same even if the current density changes.

A noticeable change in the activation resistance is recorded when the current density is swept. At low current densities a high activation resistance is measured. The activation resistance decreases as the current density increases. The effect is described as the reaction needs a certain amount of energy to drive it. At low current densities, when a small amount of electrons is present a larger resistance is present to drive $2H_2O \rightarrow 4H^+ + O_2 + 4e^-$ reaction. At high current densities this resistance that drives the reaction is smaller. The activation resistance decreased from 10.29 mΩ to 1.31 mΩ as the current density increased from 0.1 A/cm^2 to 1.1 A/cm^2. The activation resistance, R_{act} is almost 10 times smaller at high current densities than at low current densities.

Operating at higher current densities decreases the activation resistance but increase the effect of mass transfer. Although only a small amount of mass transfer effect is noticeable at the high current density after the semicircle. The Warburg parameter decreased from 1408 k$Ss^{0.5}$ to 4.06 k$Ss^{0.5}$ as the current density increased from 0.1 A/cm^2 to 1.1 A/cm^2. A smaller value of the Warburg parameter indicates a larger amount of mass transfer occurring. A Warburg value of less than 1 k$Ss^{0.5}$ can have a limiting performance effect due to mass transfer. The Warburg value of 4.06 k$Ss^{0.5}$ is

concern as regards to the optimal operating point because mass transfer is occurring. In figure 6.9 the ohmic, activation and mass transfer losses were normalised to illustrate the losses at different current densities.

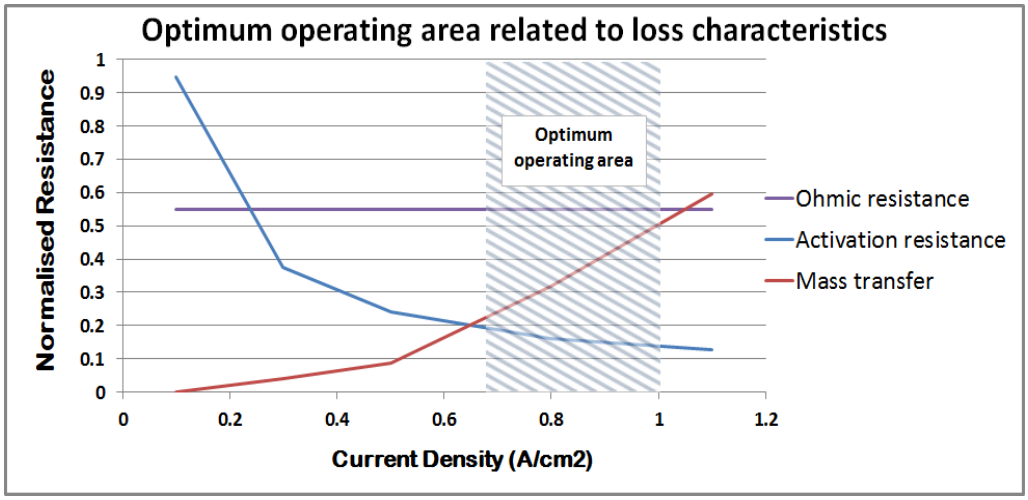

Figure 6.9: Optimum operating area related to loss characteristics

The optimum operating area is shown in figure 6.9. The ohmic resistance is constant over the whole current density range. The activation resistance decreases as the current density increases. An optimum point of operation is achieved when the activation resistance is smaller than 0.2 (normalised). The effect of mass transfer limits the current density. A Warburg parameter of less than 0.5 (normalised) is desirable. The optimum operating area is between 0.7 A/cm^2 and 1 A/cm^2.

6.4 Characterisation of components

In this section the effect of gas diffusion media on the performance of the PEM electrolyser is investigated. The function of the GDLs are to transport the reactants and products to and from the electrode-membrane interface.

The single cell PEM electrolyser was operated at 60 °C and at atmospheric pressure. The same MEA and PEM electrolyser hardware were used in both experimental procedures. Two different anode GDLs (where the oxygen evolution reaction (OER) occurs) were used. The Nyquist plots of both the GDL A and GDL B is shown in figure

6.10 and 6.11. The current density was varied from low to high to investigate the effect of the GDL on the performance of the PEM electrolyser.

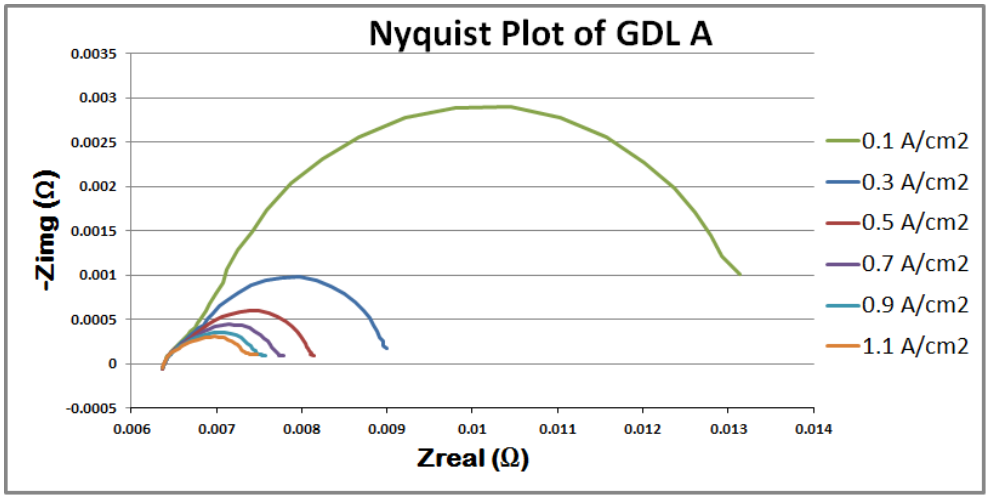

Figure 6.10: Nyquist plot of GDL A

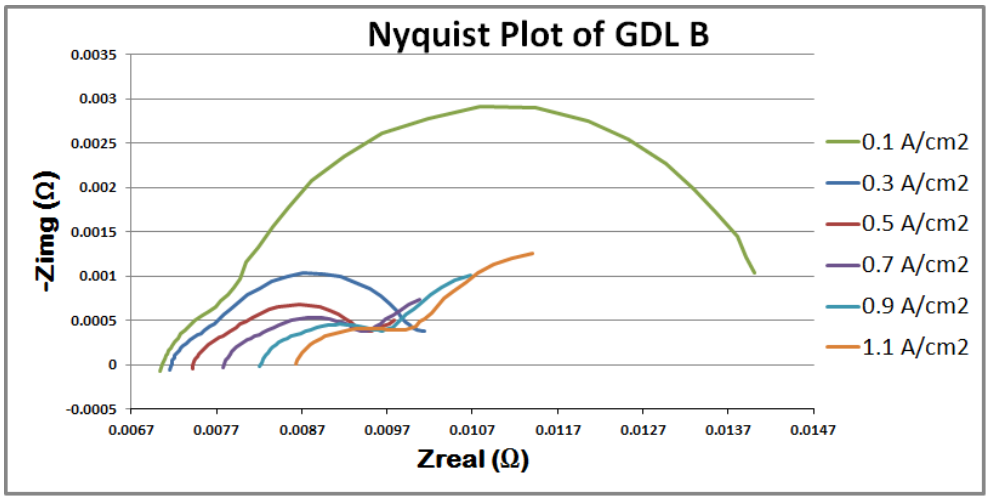

Figure 6.11: Nyquist plot of GDL B

6.4.1 Ohmic resistance

The resistances associated with a GDL includes several different components. The contact resistance between the GDL and current collector plates, the contact resistance between the GDL and the electro-catalyst and the resistance of the GDL itself. The ohmic resistance is obtained at the intercept of the impedance with the real axis on the

high frequency side. The equivalent circuit model was fitted to the experimental EIS data and the ohmic resistance parameter, R_{ohm} at different current densities for both GDLs is shown in table 6.3.

Table 6.3: Ohmic resistance of the GDL A and GDL B

	R_{ohm} of GDL A (mΩ)	R_{ohm} of GDL B (mΩ)
0.1 A/cm^2	6.36	7.04
0.3 A/cm^2	6.37	7.15
0.5 A/cm^2	6.37	7.42
0.7 A/cm^2	6.37	7.78
0.9 A/cm^2	6.37	8.21
1.1 A/cm^2	6.37	8.63

The ohmic resistance parameter of the equivalent circuit model for GDL A stays the same at 6.37 mΩ for all the current densities. The ohmic resistance parameter of the equivalent circuit model for GDL B increases as the current density increases. This increasing ohmic resistance can only be due to the GDL. The resistance between the GDL B and current collector plates, the contact resistance between the GDL B and the electro-catalyst and the resistance of the GDL B itself increases as the current density increases. The ohmic resistance effect of GDL B is not desirable in a PEM electrolyser.

6.4.2 Mass transfer effect

Mass transfer limitation regarding the anode GDL will occur due to insufficient reactant supply to the electrode/membrane interface. The effect can be noticed as a 45° line following the first semicircle at low frequencies in the Nyquist plot in figure 6.11. The equivalent circuit model was fitted to the experimental EIS data and the

Warburg parameter at different current densities for GDL B is shown in table 6.4.

Table 6.4: Warburg parameter for GDL B

	Warburg parameter of GDL B ($Ss^{0.5}$)
0.1 A/cm^2	822e3
0.3 A/cm^2	7803
0.5 A/cm^2	1797
0.7 A/cm^2	985.2
0.9 A/cm^2	645.9
1.1 A/cm^2	489.3

The Warburg parameter decreases as the current density increases. A small Warburg parameter value indicates a large mass transfer effect. The 45° line starts to occur at current densities higher than 0.7 A/cm^2 with a Warburg parameter less than 1000. The mass transfer effect of GDL B is not desirable in a PEM electrolyser.

6.5 Conclusion

The validation of the equivalent circuit model is done in three sections. The ability of the equivalent circuit model to characterise multiple MEAs with different electrochemical properties. Identifying the optimum operating area. Characterising hardware components of the PEM electrolyser.

The three MEAs with different electro-catalysts were investigated. The equivalent circuit model was fitted to the experimental EIS data. The parameters associated with the losses were analysed. The ohmic losses of the three MEAs were more or less the same. The same membrane thickness was used in all three of the MEAs and the

difference in ohmic resistance can be related to the resistance of the electro-catalysts. The activation resistance of supplier A is high and causes the high overpotential. The mass transfer effect on all three MEAs were negligible.

The optimum operating area was investigated by identifying the losses at different current densities. The optimum operating area is usually identified using the polarisation curve by specifying a maximum overpotential. In this study the losses are identified at the current density. The severity of the loss is calculated and the optimum operating area is identified.

The MEAs are the most important part of the PEM electrolyser. The hardware of the PEM electrolyser is sometimes forgotten but with EIS the effect of the hardware components can be characterised. Two different GDLs are characterised and the one with the best performance was identified.

CHAPTER 7

CONCLUSIONS

7.1 Introduction

This chapter concludes the dissertation with an overview of the work done with reference to the characterisation of a PEM electrolyser. The valuable attributes and shortcomings of the EIS method are discussed. Recommendations are made for future work in the area of characterising a PEM electrolyser.

7.2 Overview

PEM electrolysers are characterised by combining electrical and chemical phenomena. It is therefore a challenging task to characterise and derive models for electrochemical systems. A number of characterisation methods exist to investigate the performance of PEM electrolysers. The EIS method has a couple of advantages above the other electrochemical methods and was selected for this study.

The PEM electrolysers have a couple of components (see figure 4.4) and different processes occur within and between these components. One advantage of EIS is the ability to distinguish between these components and processes. Other advantages are

that the technique can be applied while the electrolyser is operating and the technique is non-invasive. The high cost of the required equipment and the time needed to acquire data at low frequencies are the disadvantages of the method.

The focus of this study was therefore to develop an equivalent circuit model which is fitted to the experimental EIS data. The parameters of the equivalent circuit model represent the components and processes of the PEM electrolyser.

7.3 Main outcomes

The outcomes of this study were discussed at the beginning of this dissertation in section 1.5. The following sections will illustrate how the outcomes were achieved.

7.3.1 Experimental procedure

The experimental procedure was successfully carried out. The graphite anode flow field was replaced with a titanium flow field to ensure the required corrosion resilience. The single cell was assembled and a test station with the needed specifications was developed.

7.3.2 Model development

The equivalent circuit model was developed and is shown in figure 7.1. The development aimed at the losses of the PEM electrolyser. The three losses are ohmic, activation and mass transfer losses.

The ohmic resistance, R_{ohm} describes the ohmic losses of the whole cell. The resistance of the conductors, membrane and the contact resistance are measured with the EIS technique. The inductance of the conductors is presented by I_{nd}.

The activation losses, R_{act} are due to the kinetics of the two reactions at the anode and cathode. The OER (oxygen evolution reaction) at the anode is slower than the HER

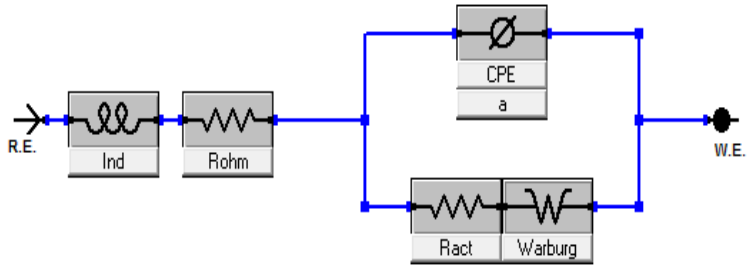

Figure 7.1: The final equivalent circuit model

(hydrogen evolution reaction) at the cathode and therefore the losses at the cathode are considered to be negligible. CPE and a are parameters of the CPE and are responsible for the shape of the semicircle. The mass transfer effect is associated with W_{arburg}.

7.3.3 Model verification and validation

The parameters of the model are generated by fitting the equivalent circuit model to the experimental EIS data with a NLLS fitting method.

The verification of the equivalent circuit model was done by verifying the results of the EIS method with other electrochemical techniques such as the polarisation curves and Tafel plots. A significant finding was made when EIS was used to investigate the ohmic resistance. Three membranes with different thickness were used and the ohmic resistances was identified with the equivalent circuit model. The values were extrapolated to a point where the thickness was zero, see section 5.2.3. This led to the important factor of separating the resistance of the membrane and catalyst layers with the use of EIS. This was only achievable when three MEAs with different thickness were used indicating one shortcoming of EIS.

The validation of the equivalent circuit model focussed on the characterisation of multiple MEAs. The MEAs were provided from different commercial suppliers having different electro-catalyst layers and loading of electro-catalyst layers. The equivalent circuit was successful to characterise all three MEAs.

Another significant contribution of EIS was indicating an operating area. The optimum

operating area is usually identified with the polarisation curve but with EIS the losses were identified to specify a more accurate operating area. The losses were monitored using the equivalent circuit model at different current densities. The optimum operating area was selected when all three losses were at a relatively minimum point as shown in figure 7.2.

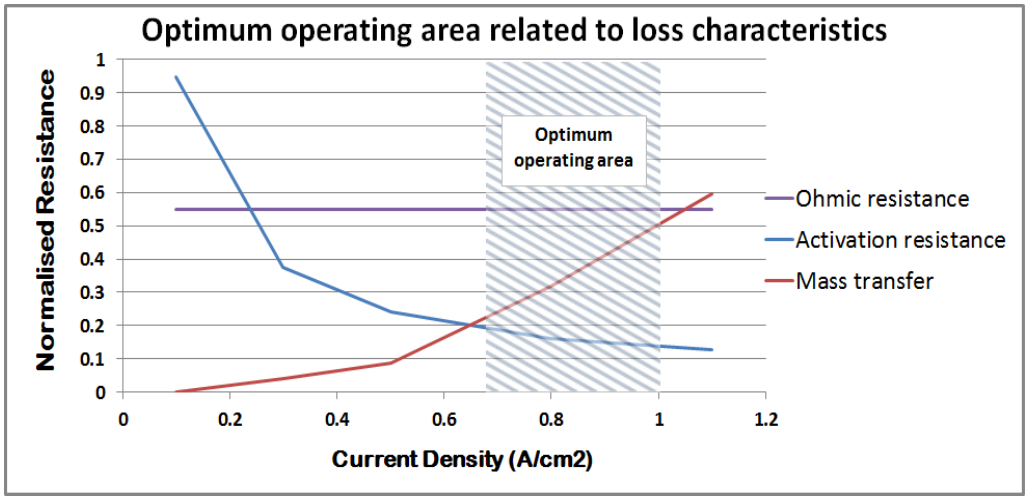

Figure 7.2: Optimum operating area

The shortcoming in this section was the critical impact of the losses. As indicated in figure 7.2 the mass transfer resistance is increasing but in the polarisation curve no performance loss is noted. Determining the critical impact of the loss can be of great value.

7.4 Recommendations and future work

The mass transfer effect can be seen as a 45° line at low frequencies on the Nyquist plot. The effect of mass transfer can also be seen on the polarisation curve but at a slightly higher current density while the mass transfer effect is noticed at lower current densities with EIS. A study can be made to determine when the mass transfer effect starts to limit the performance of the electrolyser. Further more a study to determine the critical point of each loss where it starts to influence the overall performance. The identification of the critical point of the loss can lead to an increase of the operating

current density.

The ability to measure the losses in a PEM electrolyser places EIS in a diagnostic tool category. The inclusion of real time evaluation could be useful to monitor the state of the electrolyser. Only a few vital frequency points can be identified and should be easily achievable.

The ohmic resistance determined by EIS is a representation of the ohmic resistance of the whole system. Current interruption is a method used to measure the resistance of the membrane. The results of these two methods can be compared to indicate the ohmic resistance of the system.

7.5 Closure

The objective to characterise a PEM electrolyser using EIS was achieved. The experimental EIS results were fitted to an equivalent circuit model. The model was evaluated with other electrochemical methods. The usefulness of the equivalent circuit model was illustrated by characterising three different MEAs with different electrochemical properties.

APPENDIX A

THEORETICAL MODELS

A.1 Gibbs free energy

Josiah Willard Gibbs defined the Gibbs free energy in 1873. This thermodynamic property predicts if a process will occur spontaneously at a constant temperature and pressure. Gibbs free energy measures the "useful" or process-initiating work obtainable from a thermodynamic system. The Gibbs free energy is defined by $G = H - TS$ where H, T and S are enthalpy, temperature and entropy respectively. A change in Gibbs free energy is represented by

$$\Delta G = \Delta H - T\Delta S \tag{A.1}$$

where ΔG is zero at equilibrium; negative for spontaneous processes and positive for non spontaneous processes. We can see from equation (A.1) the chemical reaction has two components:

1. ΔH is the drive toward stability. The products are more stable than the reactants if $\Delta H < 0$.

2. ΔS is the drive to disorder. The products are more disordered than the reactants if $\Delta S > 0$.

In a chemical reaction ΔH and ΔS is independent of each other. If they have the same sign they are working against each other. To make the entropy overrule, an increase in the temperature is needed or to make the enthalpy overrule a decrease in the temperature is needed [53].

An electrochemical reaction is expressed in equation (A.2). This electrochemical reaction will be used throughout the illustration of the method. O is the reactant and R is the product.

$$O + ne^- \rightarrow R \tag{A.2}$$

The Gibbs free energy can be written as:

$$\Delta G = \Delta G^0 + RT \ln \frac{[R]}{[O]} \tag{A.3}$$

where ΔG^0 is the standard free energy, $[R]$ is the activity of the product and $[O]$ is the activity of the reactant at equilibrium. R is the ideal gas constant and T is the temperature in kelvin.

A.2 Nernst equation

An electrolyser adds a new phenomena, electrical energy to the thermodynamics. A new fundamental study of thermodynamics is necessary. A new form of energy, dw_{elec} is added to form

$$dU = TdS - pdV + dw_{elec}. \tag{A.4}$$

The Lagendre transformation is applied to obtain the Gibbs free energy to give

$$G = U + pV - Ts, \tag{A.5}$$

thus

$$dG = -SdT + Vdp + dw_{elec}. \tag{A.6}$$

For a process at constant temperature and pressure,

$$dG = dw_{elec} \tag{A.7}$$

To convert the work from physical work, force (F) times distance (dx), to electrical work, the work is an electrical field E on a charge Q.

$$dw_{elec} = Fdx = QE(x)dx \tag{A.8}$$

It is known for an electric field to be a derivative of electrical potential ψ,

$$dw_{elec} = Q\frac{d\psi}{dx}dx = -Qd\psi \tag{A.9}$$

$$w_{elec} = \int -Qd\psi = -Q\int d\psi = -QE. \tag{A.10}$$

It is more convient to use moles of electrons rather than individual electrons. Thus,

$$Q = -nF \tag{A.11}$$

The Gibbs free energy equation:

$$\Delta G = -nFE \tag{A.12}$$

Equation (A.12) is the fundamental equation of electrochemistry because it relates the electromotive force of an electrochemical cell to the thermal properties of the chemical reaction carried out in that cell

$$E = E^0 + \frac{RT}{nF}\ln\frac{[O]}{[R]} \tag{A.13}$$

where E^0 is the standard thermodynamic potential at 25 °C.

The electrochemical reaction in a fuel cell and electrolyser involve gases. The pressure of the gases will have an effect on the electrode potential.

The reaction for a fuel cell at the anode is

$$H_2 \rightarrow 2H^+ + 2e^-. \tag{A.14}$$

Therefore electrode potential at the anode is

$$E_a = E_a^0 + \frac{RT}{2F}\ln\frac{[H^+]^2}{P_{H_2}}, \tag{A.15}$$

and the reaction at the cathode is:

$$O_2 + 4H^+ + 4e^- \rightarrow 2H_20. \tag{A.16}$$

Therefore electrode potential at the cathode is

$$E_c = E_c^0 - \frac{RT}{4F} \ln \frac{[H_2O]}{P_{O_2}[H^+]^4}. \tag{A.17}$$

The Nernst equation for a electrolyser can be derived with the reaction at the anode

$$2H_2O \rightarrow 4H^+ + O_2 + 4e^-. \tag{A.18}$$

Therefore electrode potential at the anode is

$$E_a = E_a^0 + \frac{RT}{2F} \ln \frac{[H^+]^4}{P_{O_2}}. \tag{A.19}$$

And the reaction at the cathode is

$$4H^+ + 4e^- \rightarrow 2H_2. \tag{A.20}$$

Therefore electrode potential at the cathode is

$$E_c = E_c^0 - \frac{RT}{4F} \ln \frac{[H_2]}{P_{H_2}[H^+]^4}. \tag{A.21}$$

P_{O_2} and P_{H_2} is the partial pressures of oxygen and hydrogen gasses. At the cathode the potential is dependant on water as an liquid. The activity of water is usually considered to be one.

The fuel cell voltage can be expressed as

$$E_{cell} = E_{cell}^0 + \frac{RT}{2F} \ln \frac{P_{H_2} P_{O_2}^{0.5}}{P_{H_2O}} \tag{A.22}$$

The Nernst equation (A.22) is a thermodynamic expression of the state of the electrochemical reaction. It can give the value of the thermodynamic electrode potential and the direction of the reaction.

Overpotential

At equilibrium in a electrochemical reaction $O + ne^- \rightarrow R$, the forward reaction rate is the same as the backward reaction rate. This implies that the overall reaction rate is zero, no net electric current is produced. The potential at equilibrium is the Nernst potential or the thermodynamic potential. To get the net current of the reaction the potential applied to the electrode should shift away from the Nernst potential and is called the overpotential:

$$\eta = E - E^0 \tag{A.23}$$

where E is the applied potential and E^0 is the Nernst potential.

Exchange Current Density

The concentrations of the reactions and products in a electrochemical reaction (A.2) at equilibrium stays the same. Although reactions are still taking place, but the forward and backward reaction rates is the same. No external current flows into the system and no current flows out of the system either. The current density inside the system is called exchange current density. The exchange current density is a kinetic parameter and it is dependant on the reaction and the electrode surface.

The magnitude of the exchange current density determines the rate of the electrochemical reaction. A small exchange current density requires a high overpotential for a high current density and a large exchange current density requires a lower overpotential for a high current density. The exchange current density for H_2 oxidation is 5 times greater than O_2 reduction, thus a high overpotential is needed at the O_2 reduction to produce the same current density as the H_2 [36].

APPENDIX B

THERMODYNAMIC EFFICIENCY

Electrical work ($\Delta GkJ.mol^{-1}$) and heat ($T\Delta S.mol^{-1}$) must be provided to perform water electrolysis.

$$\Delta G(>0) = \Delta H(>0) - T\Delta S(>0) \tag{B.1}$$

The water heat of dissociation is

$$\Delta H = \Delta G + T\Delta S = +286.02kJ.mol^{-1} \tag{B.2}$$

and the entropy change is

$$\Delta S = S_F(H_2) + 0.5S_F(O_2) - S_F(H_2O) = +0.163285kJ.mol^{-1} \tag{B.3}$$

the heat required at 298K is $T\Delta S = +48.68kJ.mol^{-1}$. The electrical work required at 298K is

$$\Delta G = +237.34kJ.mol^{-1} \tag{B.4}$$

The minimum amount of energy required must be equal to the free enthalpy change $\Delta G(>0) = +nFE$. n is number of electrons exchanged during the electrochemical process. F is the Faraday constant.E is thermodynamic voltage (equilibrium) applied to the cell at zero current. ΔG is the Gibbs energy change associated to the

electrochemical reaction. For $\Delta G > 0$ the process is non-spontaneous and for $\Delta G < 0$ the process is spontaneous.

In standard temperature and pressure conditions the Gibbs energy change is

$$\Delta G = +237.22 kJ.mol^{-1}, \tag{B.5}$$

thus the voltage is

$$E = \frac{\Delta G}{2F} = 1.23V. \tag{B.6}$$

The water heat dissociation is

$$\Delta H = +285.840 kJ.mol^{-1}, \tag{B.7}$$

thus the voltage

$$E = \frac{\Delta H}{2F} = 1.48V \tag{B.8}$$

Hydrogen lower heating value (LHV) is equal to 1.23V and the HHV is 1.48V.

BIBLIOGRAPHY

[1] S. Ahmed, A. Jaber, M. Konukiewitz, R. Dixon, M. Eckhart, D. Hales, and G. Thompson, "Renewables 2011," 2011.

[2] J. Cargnelli, "Alkaline and PEM Electrolyzer Development," Potchefstroom, South Africa, 2012.

[3] S. Grigoriev, V. Porembsky, and V. Fateev, "Pure hydrogen production by PEM electrolysis for hydrogen energy," *International Journal of Hydrogen Energy*, vol. 31, no. 2, pp. 171–175, Feb. 2006. [Online]. Available: http://linkinghub.elsevier.com/retrieve/pii/S036031990500145X

[4] A. J. Bard, L. R. Faulkner, E. Swain, and C. Robey, *Electrochemical methods. Fundamentals and Applications*, second edi ed.

[5] K. W. Energy, "Key World Energy," *Statistics*, 2010.

[6] P. Beach, "Towards a Hydrogen Economy," no. 5, 2005.

[7] C. Hebling, E. Ojong, and S. Rau, "The Role of Hydrogen as a Fuel for Future Mobility and a Storage Media in a Renewable Energy Economy," Potchefstroom, South Africa, p. 86, 2012.

[8] E. Anderson, "PEM Electrolyzer Development," Potchefstroom, South Africa, p. 49, 2012.

[9] B. G. Pollet, I. Staffell, and J. L. Shang, "Current status of hybrid, battery and fuel cell electric vehicles: From electrochemistry to market prospects," *Electrochimica Acta*, pp. 1–15, 2012. [Online]. Available: http://dx.doi.org/10.1016/j.electacta.2012.03.172

[10] F. M. Oberlin R, "Status of the membral process for water electrolysis," *Hydrogen energy progress VI, proceedings of the sixth world hydrogen energy conference*, pp. 333–400, 1986.

[11] R. G. Cawthorn, "The platinum and palladium resources of the Bushveld Complex," *South African Journal Of Science*, no. December, pp. 481–489, 1999.

[12] J. Wu, X. Zi, H. Wang, M. Blanco, J. J. Martin, and J. Zhang, "Diagnostic tools in PEM fuel cell research : Part I Electrochemical techniques," vol. 33, pp. 1735 – 1746, 2008.

[13] G. F. C. Rogers and Y. R. Mayhew, *Engineering Thermodynamics: Work and Heat Transfer*, 4th ed. London: Longman, 1992.

[14] Y. A. Cengel and M. A. Boles, *Thermodynamics: An Engineering Approach*, 4th ed. New York: McGraw-Hill, Inc, 2002.

[15] A. Valero, A. Valero, and P. Vieillard, "The thermodynamic properties of the upper continental crust : Exergy , Gibbs free energy and enthalpy," *Energy*, pp. 1–7, 2011. [Online]. Available: http://dx.doi.org/10.1016/j.energy.2011.06.012

[16] H. Xi, J. Sun, and V. Tsourapas, "A control oriented low order dynamic model for planar SOFC using minimum Gibbs free energy method ," *Direct*, vol. 165, pp. 253–266, 2007.

[17] A. Lima and I. L. Müller, "Operation of solid oxide fuel cells on glycerol fuel : A thermodynamic analysis using the Gibbs free energy minimization approach," vol. 195, pp. 5637–5644, 2010.

[18] S. Edition and W. Virginia, *Fuel Cell Handbook*, 2004, no. November.

[19] F. Barbir, *PEM Fuel Cells*. New York: Elsevier, 2005.

[20] M. A. Rubio, A. Urquia, and S. Dormido, "PEM Fuel Cell Diagnostic Tools, Chapter 6: Current Interuption," 2011, pp. 101–127.

[21] P. G. Bruce and F. R. S. Frse, "The Power of Electrochemical Impedance Techniques," *Corrosion*, no. August, 2008.

[22] P. Costamagna, "Transport phenomena in polymeric membrane fuel cells," *Chemical Engineering Science*, vol. 56, no. 2, pp. 323–332, Jan. 2001. [Online]. Available: http://linkinghub.elsevier.com/retrieve/pii/S0009250900002323

[23] W. Mérida, D. Harrington, J. Le Canut, and G. McLean, "Characterisation of proton exchange membrane fuel cell (PEMFC) failures via electrochemical impedance spectroscopy," *Journal of Power Sources*, vol. 161, no. 1, pp. 264–274, Oct. 2006. [Online]. Available: http://linkinghub.elsevier.com/retrieve/pii/S0378775306005982

[24] T. J. Freire and E. R. Gonzalez, "Effect of membrane characteristics and humidification conditions on the impedance response of polymer electrolyte fuel cells," *Journal of Electroanalytical Chemistry*, vol. 503, no. 1-2, pp. 57–68, Apr. 2001. [Online]. Available: http://linkinghub.elsevier.com/retrieve/pii/S0022072801003643

[25] B. Andreaus, "Analysis of performance losses in polymer electrolyte fuel cells at high current densities by impedance spectroscopy," *Electrochimica Acta*, vol. 47, no. 13-14, pp. 2223–2229, May 2002. [Online]. Available: http://linkinghub.elsevier.com/retrieve/pii/S0013468602000592

[26] J. Song, S. Cha, and W. Lee, "Optimal composition of polymer electrolyte fuel cell electrodes determined by the AC impedance method," *Journal of Power Sources*, vol. 94, no. 1, pp. 78–84, Feb. 2001. [Online]. Available: http://linkinghub.elsevier.com/retrieve/pii/S0378775300006297

[27] M. Eikerling and a.a Kornyshev, "Electrochemical impedance of the cathode catalyst layer in polymer electrolyte fuel cells," *Journal of Electroanalytical Chemistry*, vol. 475, no. 2, pp. 107–123, Oct. 1999. [Online]. Available: http://linkinghub.elsevier.com/retrieve/pii/S0022072899003356

[28] A. Marshall, B. Brresen, G. Hagen, M. Tsypkin, and R. Tunold, "Hydrogen production by advanced proton exchange membrane (PEM) water electrolysers–Reduced energy consumption by improved electrocatalysis," *Energy*, vol. 32, no. 4, pp. 431–436, 2007. [Online]. Available: http://www.sciencedirect.com/science/article/B6V2S-4KXDWCB-1/2/1c5a15bcd327f1e075c16d232be9caec

[29] P. Choi, "A simple model for solid polymer electrolyte (SPE) water electrolysis," *Solid State Ionics*, vol. 175, no. 1-4, pp. 535–539, Nov. 2004. [Online]. Available: http://linkinghub.elsevier.com/retrieve/pii/S0167-2738(04)00642-3

[30] F. Marangio, M. Santarelli, and M. Cali, "Theoretical model and experimental analysis of a high pressure PEM water electrolyser for hydrogen production," *International Journal of Hydrogen Energy*, vol. 34, no. 3, pp. 1143–1158, Feb. 2009. [Online]. Available: http://linkinghub.elsevier.com/retrieve/pii/S0360319908016571

[31] H. Gorgun, "Dynamic modelling of a proton exchange membrane (PEM) electrolyzer," *International Journal of Hydrogen Energy*, vol. 31, no. 1, pp. 29–38, Jan. 2006. [Online]. Available: http://linkinghub.elsevier.com/retrieve/pii/S0360319905000868

[32] N. Dale, "Characterization of PEM electrolyzer and PEM fuel cell stacks using electrochemical impedance spectroscopy," Ph.D. dissertation, 2001. [Online]. Available: http://gradworks.umi.com/33/83/3383390.html

[33] E. Barsoukov and J. R. Macdonald, *Impedance spectroscopy: theory, experiment, and applications*, second edi ed., E. Barsoukov and J. R. Macdonald, Eds. John Wiley & Sons, Inc., 2005.

[34] R. A. Latham, "Algorithm Development for Electrochemical Impedance Spectroscopy Diagnostics in PEM Fuel Cells," *Change*, 2004.

[35] N. Wagner, "Characterization of membrane electrode assemblies in polymer electrolyte fuel cells using a.c. impedance spectroscopy," *Journal of Applied Electrochemistry*, vol. 32, no. 8, pp. 859–863, 2002.

[36] X.-Z. Yuan, C. Song, H. Wang, and J. Zhang, *Electrochemical Impedance Spectroscopy in PEM Fuel Cells*. London: Springer London, 2010. [Online]. Available: http://www.springerlink.com/index/10.1007/978-1-84882-846-9

[37] R. O'Hayre, S.-W. Cha, W. Colella, and F. B.Prinz, *Fuel Cel Fundamentals*, second edi ed. Wiley, 2009.

[38] A. M. Dhirde, S. Member, N. V. Dale, H. Salehfar, S. Member, M. D. Mann, and T.-h. Han, "Equivalent Electric Circuit Modeling and Performance Analysis of a PEM Fuel Cell Stack Using Impedance Spectroscopy," *Energy*, vol. 25, no. 3, pp. 778–786, 2010.

[39] S. A. Ivers-Tiffe e E, Weber A, *Handbook of fuel cells: fundamentals, technology and applications*, volume 2 ed., W. Vielstich, H. Gasteiger, and A. Lamm, Eds. Wiley, 2003.

[40] B. Andreaus and G. G. Scherer, "Proton-conducting polymer membranes in fuel cells humidification aspects," *Solid State Ionics*, vol. 168, pp. 311 – 320, 2004.

[41] N. Wagner and E. Gülzow, "Change of electrochemical impedance spectra (EIS) with time during CO-poisoning of the Pt-anode in a membrane fuel cell," *Journal of Power Sources*, vol. 127, no. 1-2, pp. 341–347, Mar. 2004. [Online]. Available: http://linkinghub.elsevier.com/retrieve/pii/S0378775303009698

[42] N. Wagner, "Change of electrochemical impedance spectra during CO poisoning of the Pt and Pt?Ru anodes in a membrane fuel cell (PEFC)," *Electrochimica Acta*, vol. 48, no. 25-26, pp. 3899–3907, Nov. 2003. [Online]. Available: http://linkinghub.elsevier.com/retrieve/pii/S0013468603005280

[43] N. Wagnerc, C. A. Schiller, F. Richter, E. Gu, T. Str, and D. Kronach, "Validation and evaluation of electrochemical impedance spectra of systems with states that change with time," *Evaluation*, pp. 374–378, 2001.

[44] N. Wagnerc, C. A. Schiller, F. Richter, and E. Gu, "Relaxation impedance as a model for the deactivation mechanism of fuel cells due to carbon monoxide poisoning," pp. 2113–2116, 2001.

[45] B. A. Boukamp, "A package for impedance/admittance data analysis," *Solid State Ionics*, vol. 19, pp. 136–140, 1986.

[46] B. Boukamp, "A nonlinear least squares fit procedure for analysis of immittance data of electrochemical systems," *Solid State Ionics*, vol. 20, pp. 31–44, 1986.

[47] P. Millet, "Water electrolysis," Potchefstroom, South Africa, p. 72, 2012.

[48] S. Slade, S. A. Campbell, T. R. Ralph, and F. C. Walsh, "Ionic Conductivity of an Extruded Nafion 1100 EW Series of Membranes," pp. 1556–1564, 2002.

[49] V. Antonucci, a. Di Blasi, V. Baglio, R. Ornelas, F. Matteucci, J. Ledesma-Garcia, L. Arriaga, and a.S. Aricò, "High temperature operation of a composite membrane-based solid polymer electrolyte water electrolyser," *Electrochimica Acta*, vol. 53, no. 24, pp. 7350–7356, Oct. 2008. [Online]. Available: http://linkinghub.elsevier.com/retrieve/pii/S0013468608005008

[50] J. Hu, "Oxygen evolution reaction on IrO2-based DSA type electrodes: kinetics analysis of Tafel lines and EIS," *International Journal of Hydrogen Energy*, vol. 29, no. 8, pp. 791–797, Jul. 2004. [Online]. Available: http://linkinghub.elsevier.com/retrieve/pii/S0360319903002465

[51] S. Siracusano, V. Baglio, a. Di Blasi, N. Briguglio, a. Stassi, R. Ornelas, E. Trifoni, V. Antonucci, and a.S. Aricò, "Electrochemical characterization of single cell and short stack PEM electrolyzers based on a nanosized IrO2 anode electrocatalyst," *International Journal of Hydrogen*

Energy, vol. 35, no. 11, pp. 5558–5568, Jun. 2010. [Online]. Available: http://linkinghub.elsevier.com/retrieve/pii/S0360319910006166

[52] A. M. Dhirde, S. Member, N. V. Dale, H. Salehfar, S. Member, M. D. Mann, and T.-h. Han, "Equivalent Electric Circuit Modeling and Performance Analysis of a PEM Fuel Cell Stack Using Impedance Spectroscopy," vol. 25, no. 3, pp. 778–786, 2010.

[53] W. R. SALZMAN, "W. R. SALZMAN WEBSITE," 2002. [Online]. Available: http://www.chem.arizona.edu/ salzmanr/480a/480ants/elecwork/elecwork.html